JGR Atmospheres

RESEARCH ARTICLE
10.1029/2024JD042588

Special Collection:
Chemistry and Climate Impacts of the Asian Summer Monsoon

Highlighting the Impact of Anthropogenic OCS Emissions on the Stratospheric Sulfur Budget With In Situ Observations

Colin Gurganus[1,2], Andrew Rollins[2], Eleanor Waxman[1,2], Laura L. Pan[3], Warren P. Smith[3], Rei Ueyama[4], Wuhu Feng[5,6], Martyn P. Chipperfield[5,7], Elliot L. Atlas[8], Joshua P. Schwarz[2], Samantha DeLone[1,2], and Troy Thornberry[2]

[1]Cooperative Institute for Research in Environmental Sciences, University of Colorado, Boulder, CO, USA, [2]NOAA Chemical Sciences Laboratory, Boulder, CO, USA, [3]Atmospheric Chemistry Observations & Modeling Laboratory, NSF National Center for Atmospheric Research, Boulder, CO, USA, [4]NASA Ames Research Center, Moffett Field, CA, USA, [5]Institute for Climate and Atmospheric Science, School of Earth and Environment, University of Leeds, Leeds, UK, [6]National Centre for Atmospheric Science, University of Leeds, Leeds, UK, [7]National Centre for Earth Observation, University of Leeds, Leeds, UK, [8]Department of Atmospheric Sciences, Rosenstiel School of Marine, Earth, and Atmospheric Science, University of Miami, Miami, FL, USA

Abstract Carbonyl sulfide (OCS) is an important atmospheric sulfur species that plays a dominant role in the formation of (nonvolcanic) stratospheric sulfate aerosol in the middle stratosphere. Major uncertainties in surface sources and sinks and inconsistent model representation of vertical transport limit understanding of OCS distribution, particularly in the sparsely sampled upper atmosphere. During the 2022 Asian Summer Monsoon Chemical and CLimate Impact Project (ACCLIP) campaign, in situ measurements of OCS in the Upper Troposphere and Lower Stratosphere (UTLS) at the eastern edge of the Asian summer monsoon anticyclone (ASM), showed significant OCS enhancements (>750 ppt) near the tropopause from convectively influenced air parcels. Here, we compare these novel Asian UTLS measurements with long-term satellite observations and regional measurements to broaden understanding of OCS trends and its transport by the ASM. Trajectory analysis identifies northern China as the main source region for deep convective lofting of OCS-enriched parcels and demonstrates ASM entrainment in the UTLS, allowing evaluation of global model predictions for OCS's stratospheric influence. The ACCLIP data set provides vital in situ validation of limited vertically resolved OCS data in a region of significant anthropogenic emissions, which serves to enhance our understanding of the global sulfur budget.

Plain Language Summary Carbonyl sulfide (OCS) is the most prevalent sulfur-containing compound in the atmosphere and plays a critical role in the formation of stratospheric sulfate aerosols, which impact the Earth's climate by reflecting solar radiation. In this study, we present novel airborne in situ measurements of OCS in the Upper Troposphere and Lower Stratosphere, collected during the 2022 ACCLIP field campaign. These measurements reveal significant OCS enhancements, exceeding 50% above the global tropospheric baseline, and are analyzed in conjunction with other in situ and remote observations, including satellite and ground-based vertical retrievals. Transport modeling confirms that the ACCLIP sampling captured outflow from northern China. Our data not only validate findings from earlier campaigns but also provide some of the first in situ evidence of rapid convective transport of OCS enhancements from the boundary layer to the tropopause. Through long-term satellite data sets, we demonstrate that efficient convective transport is a recurrent seasonal phenomenon in the region, yet it remains underrepresented in global models. These findings indicate that the stratospheric sulfur budget may be underestimated due to the insufficient representation of the rapid uplift of anthropogenic OCS emissions into the stratosphere.

Key Points:

- This study details a new in situ data set for carbonyl sulfide measurements in the upper troposphere/lower stratosphere
- Significant carbonyl sulfide enhancements near the tropopause are associated with convective lifting of anthropogenic emissions from China
- In situ data confirm that global models fail to capture the magnitude of vertical transport during the Asian summer monsoon anticyclone

Supporting Information:

Supporting Information may be found in the online version of this article.

Correspondence to:

C. Gurganus,
colin.gurganus@noaa.gov

Citation:

Gurganus, C., Rollins, A., Waxman, E., Pan, L. L., Smith, W. P., Ueyama, R., et al. (2025). Highlighting the impact of anthropogenic OCS emissions on the stratospheric sulfur budget with in situ observations. *Journal of Geophysical Research: Atmospheres*, *130*, e2024JD042588. https://doi.org/10.1029/2024JD042588

Received 30 SEP 2024
Accepted 10 APR 2025

Author Contribution:

Software: Samantha DeLone

1. Introduction

Carbonyl sulfide (OCS) plays a pivotal role in the atmosphere due to its involvement in various biogeochemical cycles and atmospheric processes. It is the most abundant sulfur-containing gas in the troposphere, significantly influencing the global sulfur budget (Montzka et al., 2007). The tropospheric concentration of OCS is governed by both natural and anthropogenic sources and sinks, including oceans, soils, wetlands, biomass burning, and industrial activities (Kettle et al., 2002). Recent studies have emphasized the need for comprehensive models to accurately simulate OCS dynamics, considering the complexities of its sources, sinks, and chemical transformations (Jernigan et al., 2022; Launois, Belviso, et al., 2015; Launois, Peylin, et al., 2015). An accurate

understanding of both OCS atmospheric abundance and transport are essential for predicting future atmospheric composition and assessing the implications for climate trends and environmental health.

OCS also plays a role in the tropospheric carbon cycle through its interaction with vegetation, with leaf uptake also acting as significant sulfur sink (J. Li et al., 2024). Plants take up OCS during photosynthesis, yet do not reemit it via respiration, making it a valuable tracer for estimating gross primary production (GPP) and understanding the carbon flux between the biosphere and the atmosphere (Berry et al., 2013). OCS can therefore be used as an effective process level measure of GPP to complement broad-scale remote sensing measures of GPP via solar-induced chlorophyll fluorescence (Parazoo et al., 2014). This dual role in both the sulfur and carbon cycles underscores the importance of OCS in the atmosphere.

Due to its significant flux and long lower stratospheric lifetime of 47 years (Karu et al., 2023), OCS is the most abundant sulfur species in the stratosphere during volcanically quiescent periods. The photolysis and oxidation of OCS in the stratosphere leads subsequently to the rapid formation of sulfuric acid (H_2SO_4), which then condenses to form sulfate aerosols, contributing to the stratospheric aerosol layer (Brühl et al., 2012). Thus, OCS plays a critical role in the global radiative balance as the primary sulfur reservoir for nonvolcanic stratospheric sulfate aerosol (Kremser et al., 2016). With a slow oxidation mechanism, OCS has a minimal contribution to lower stratospheric aerosol in the tropics and midlatitudes (<25 km), yet it is rapidly photolyzed in the middle stratosphere to form sulfate aerosol precursors. The modeled peak sulfate aerosol mass mixing ratio (~2,000 ng/kg) occurs near the 250 ppb N_2O contour (Figure 1d) as a result of OCS depletion (Figure 1b) in the absence of any other significant sulfur source, specifically SO_2 below the 20 mB level (Figure 1c) during a volcanically quiescent period. This process is critical for the maintenance of the stratospheric aerosol layer, which influences Earth's radiation budget and participates in heterogeneous chemical reactions affecting ozone depletion (Crutzen, 1976).

Despite decades of research into the stratospheric aerosol processes, understanding of the stratospheric sulfur budget is primarily derived from chemical models driven by laboratory parameterizations due to a paucity of OCS data for validation. Long-period averaging of the ACE-FTS remote sensing data set (Boone et al., 2023) confirms that OCS photolysis occurs over a narrow band at ~27 km in the tropical pipe (Figure 1a) in the same region of the maximum sulfate aerosol mixing ratio near the 250-ppb N_2O contour (Figure 1d). Due to stratospheric dynamics, air parcels only reach the OCS photolysis level by vertical transit though the isolated tropical pipe region (20N–20S) above the tropopause (Plumb, 1996). However, there is limited availability of vertically resolved remote sensing data in this equatorial region and no balloon or aircraft in situ data to validate remote retrievals within the tropical pipe. Limited stratospheric observations therefore impede our understanding of the stratospheric sulfur budget, highlighting the need for additional OCS measurements to better establish a baseline for sulfate aerosol formation. The importance of additional measurements in the upper atmosphere is critical given the increasing likelihood of perturbations induced by stratospheric aerosol injection (SAI) implementation as a climate mitigation strategy in the coming decades.

In this study, we leverage in situ OCS observations to gain deeper insights into the role of vertical transport in linking tropospheric OCS trends with the stratospheric sulfur budget. Section 2 outlines the tropospheric OCS trends and the role of vertical transport. Section 3 introduces a new data set from the 2022 Asian Summer Monsoon Chemical and CLimate Impact Project (ACCLIP) campaign, highlighting its objectives, airborne sampling methodologies, and relevant surface measurements from the study region. In Section 4, trajectory analysis is used to trace the origins of air parcels containing enhanced OCS concentrations and determine their likelihood for transport into the lower stratosphere. Section 5 compares ACCLIP in situ OCS profiles with those from ground- and satellite-based remote sensing platforms, providing an evaluation of current vertically resolved observational methods. This section also examines limitations in the representation of observed regional OCS enhancements in global chemistry models. Finally, Section 6 concludes with a broader discussion on the implications of these findings for the global sulfur budget.

2. Background and Context

2.1. Tropospheric Trends

OCS is only continually measured in the troposphere via a few global fixed sites; these include the NOAA Global Monitoring Laboratory (GML) Long-term Observations of Greenhouse gases and Ozone-depleting Substances

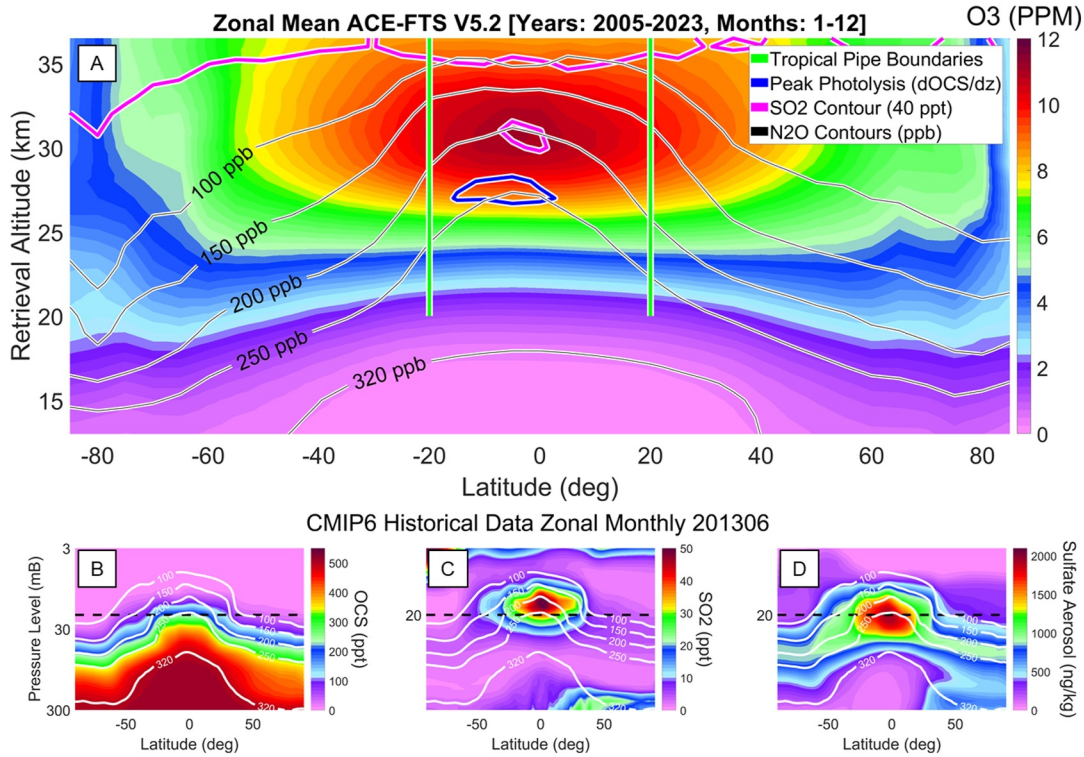

Figure 1. Visualizations of the stratospheric sulfur budget from ACE-FTS (V5.2) remote sensing profiles (a), and chemical model parameterizations (b, c, and d) overlaid with contours showing the isopleths of the N_2O mixing ratio (ppbv) as white lines to indicate for stratospheric dynamics. The N_2O distribution in the stratosphere is a good proxy for the age of air (Andrews et al., 2001). The approximate tropical pipe region (20S–20 N) is highlighted with green vertical lines. The peak in observed OCS depletion (dOCS/dZ) occurs at ~27 km in the equatorial region as a result of short-wavelength photolysis (Panel a, blue contour). In the bottom panels, a month zonal mean for the primary stratospheric sulfur budget constituents (OCS, SO_2 and sulfate aerosol) during a volcanically quiescent period (June 2013, ~2 years after the Nabro eruption) derived from a Coupled Model Intercomparison Project (CMIP6) historical run is presented. The model-estimated stratospheric sulfate aerosol maximum of ~2,000 ng S/kg aerosol occurs in the tropical pipe near the 250-ppb N_2O contour (~20 mB) with no other significant sulfur source aside from OCS (panel d). The modeling was done with CMIP6 historical simulation with Community Earth System Model version 2 (CESM2 (Danabasoglu et al., 2020)) with Whole Atmosphere Community Climate version 6 model (WACCM6 (Gettelman et al., 2019)) as its atmospheric component with a full tropospheric-stratospheric-mesospheric-lower thermosphere chemistry scheme (TSMLT), as used and described by Davis et al., 2023.

(LOGOS) network and the NASA Advanced Global Atmospheric Gases Experiment (AGAGE) networks as well as via remote sensing Fourier transform infrared (FTIR) profiles from the Network for the Detection of Atmospheric Composition Change (NDACC) network. Northern Hemisphere sample sites report a fairly consistent seasonal cycle with a minimum in late summer (Figure 2b) due to uptake by flora in the terrestrial biosphere (Montzka et al., 2007). Despite several decades of observations, the paucity of measurements in many regions of the globe, particularly Asia (Figure 2a), limits our understanding of OCS emissions from oceanic and anthropogenic sources.

Asian anthropogenic OCS emissions are estimated to be some of the most significant globally especially given the continued reduction from other regions (Campbell et al., 2015). Several short-term measurement campaigns in Asia have highlighted the significance of OCS emissions from northern China via trajectory modeling in addition to isotopic signatures (Hattori et al., 2020) and emission ratios (Blake et al., 2004). Continuous monitoring is now coming online with several AGAGE network sites in the region with the ability to sample OCS, though many of these records are not yet widely available. Anthropogenic Chinese OCS emissions were estimated to have risen ~7.2% annually from 2010 to 2015 (Y. Yan et al., 2019), which coincides with the period of steady increase in global mean lower atmosphere OCS abundance in the NOAA GML data (Figure 2a). Despite these trends, it is difficult to determine the contribution of Asian OCS emissions of the global sulfur budget based on existing sparse sampling and imperfect emissions estimates.

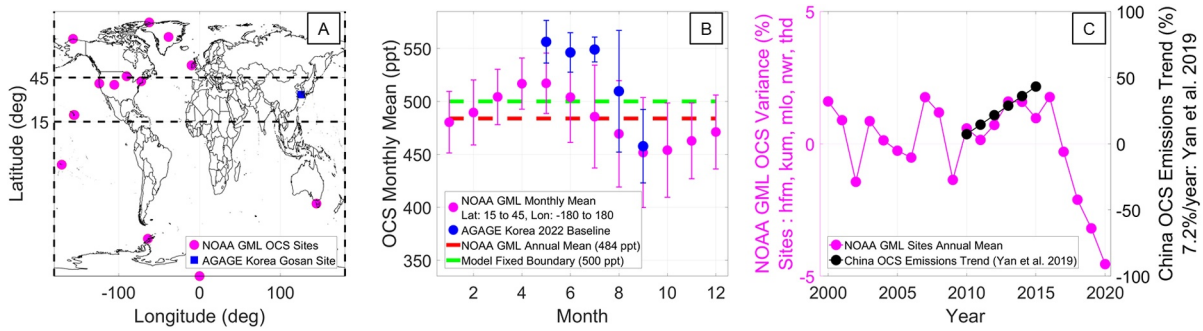

Figure 2. Boundary layer OCS trends. Panel (a): distribution of NOAA Global Monitoring Laboratory (GML) OCS boundary layer midlatitude (15–45 N) measurement sites considered for this analysis (hfm: Harvard Forest, USA, kum: Cape Kumukhai, USA, mlo: Mauna Loa, USA, nwr: Niwot Ridge, USA, thd: Trinidad Head, USA). Panel (b) shows a comparison of Northern Hemisphere midlatitude (15–45 N) monthly variation in OCS abundance from the NOAA GML 2001 to 2021 data set (Hu et al., 2021) overlaid with the 2022 Advanced Global Atmospheric Gases Experiment (AGAGE) Gosan (Korea) site baseline measurements (see Section 3 for AGAGE data set details). Note the very large enhancements in the 2022 AGAGE Korea measurements (blue) relative to the NOAA GML Northern Hemisphere mean (magenta) during the summer months. Also note that the 500-ppt fixed boundary assumption (green line) completely neglects the strong seasonal variability of the measured OCS signals. Panel (c): an annual variance from the NOAA GML archive mean in magenta, compared with the estimated China OCS emissions increase from 2010 to 2015 in black (Y. Yan et al., 2019).

After a prolonged period of increasing stratospheric OCS concentrations (2008–2016), recent NDACC network stratospheric data suggest a steady decrease in global OCS concentrations, though the magnitude of the decreasing trend is difficult to quantify (Hannigan et al., 2022). A similar pattern of decreasing global OCS has been noted in the ground-based NOAA GML data set (Belviso et al., 2022; Serio et al., 2023), and is pronounced in both in the midlatitude mean (Figure 2c) and individual measurement sites (Figure S2 in Supporting Information S1). Recent introduction of more efficient industrial CS_2 processes in general (Elliot Campbell personal communication) and a reduction of industrial VOC emissions in China specifically (Simayi et al., 2022) since 2016 may contribute to the recent reduction in OCS global atmospheric abundance. The consistency of this decreasing trend across all layers of the atmosphere may suggest a long-term change in the global sulfur budget, which has implications for the global radiative balance from a reduction in stratospheric sulfate aerosol.

Consequences of long-term variations in the global sulfur budget require a holistic consideration of the atmosphere, which can only be achieved through modeling. Many global chemical models (e.g., CESM2, WACCM, and SOCOL) are typically implemented with a fixed global surface boundary condition for OCS, which results in an assumption of a homogenous tropospheric OCS mixing ratio, typically 500 ppt (Sheng et al., 2015). Under this simplified scenario, global atmospheric dynamics produce a large flux across the tropical tropopause (300–400 Gg S/year) balanced by significant subsidence at higher latitudes (Kremser et al., 2016) resulting in a net annual flux of 30–40 Gg S/year (Feinberg et al., 2019; Sheng et al., 2015) entering the tropical pipe. However, this assumption does not capture the seasonal or long-terms trends, and likely results in a global overestimate of tropospheric OCS abundance (green line in Figure 2b).

2.2. Vertical Transport

In the free troposphere, the distribution of OCS is primarily governed by transport processes, given the limited availability of sources and sinks. Observed inhomogeneity in tropospheric abundance, particularly in the free troposphere, is largely attributed to the vertical transport of air parcels from the boundary layer. Deep atmospheric convection plays a crucial role in this vertical transport, particularly by lifting parcels into the Upper Troposphere and Lower Stratosphere (UTLS). This process is especially effective for OCS due to its relatively low Henry's law constant of approximately 2×10^{-4} mols/m^{3}Pa, which is similar in magnitude to that of carbon dioxide (Sander, 2023). The low solubility of OCS in water, as indicated by its Henry's law constant, facilitates its efficient upward transport during convective events.

Deep convection has been demonstrated to produce rapid (hours–days) stratospheric injection of lower tropospheric air parcels, which is an important stratospheric transport pathway for short-lived species (Pan et al., 2024). Alternatively, upper troposphere-injected parcels that become entrained in the core of the Asian summer monsoon anticyclone (ASM) (see Section 3.1 for more details of ASM) may undergo diabatic heating to slowly ascend and cross the tropopause (~380 K) in less than one month (Legras & Bucci, 2020). In the case of OCS, the latter

mechanism is more relevant for stratospheric transport given its long chemical lifetime. For stratospheric sulfate aerosol formation, the height of the convective injection is also important as Yan et al. suggest a twofold increase in tropical pipe transport efficiency for parcels injected above 370-K potential temperature in the ASM compared with those injected lower in the UTLS (X. Yan et al., 2019). However, accurately parameterizing vertical transport in global models remains a significant challenge, due to the complex temporal and spatial scales associated with convection.

3. UTLS Measurements and Transport

Decoupling the roles of emissions and vertical transport for the stratospheric OCS burden requires a more comprehensive in situ data set for validation. In this work, we present in situ UTLS measurements of OCS which were collected during the 2022 Asian Monsoon Chemical and CLimate Impact Project (ACCLIP) campaign. This analysis confirms OCS emissions from China, as well as the interaction of convectively lofted OCS parcels and regional atmospheric dynamics, practically the ASM. This new data set provides a touchstone for model and satellite validation of this significant stratospheric sulfur transport pathway.

3.1. ACCLIP Campaign (2022)

The ASM facilitates the uplift of boundary layer air, rich in pollutants and water vapor, to higher altitudes where these constituents can influence atmospheric composition and climate on a broader scale. This anticyclone is a dominant climatic phenomenon in the Northern Hemisphere, significantly influencing weather patterns, hydrology, and atmospheric composition. The ASM typically forms in late spring, and persisting through summer into early autumn and encompassing a significant portion of the Asian continent, its core is typically located over the Tibetan Plateau, and its influence extends from the Arabian Sea in the west to the western Pacific Ocean in the east (Hoskins & Rodwell, 1995). The ASM extends vertically from the middle to the upper troposphere and reaches into the lower stratosphere, with the spatial extent defined by an elevated tropopause height (Pan et al., 2016), making it a crucial conduit for vertical transport of air masses and chemical species from a region of high anthropogenic emissions (Randel et al., 2010). The ACCLIP campaign was conceived as a comprehensive field campaign aimed at elucidating the complex interactions between the ASM and atmospheric chemistry (Pan et al., 2022). The mission's primary objective was to investigate the transport of chemical species from the Earth's surface to the UTLS during the monsoon season, with some of the first in situ UTLS measurements on the eastern edge of the ASM.

During an intensive sampling period in summer 2022, two research aircrafts (NASA WB-57 and NSF GV), balloon platforms, and ground-based platforms conducted detailed atmospheric profiling with an operational base in Osan, Korea. This work focuses on data collected onboard the NASA WB-57 high-altitude research aircraft, the only platform to collect in situ OCS data during the campaign. In addition to scientific research flights conducted from August 2 to August 31, in situ trace gas data were also collected during test and transit flights from the WB-57's base at NASA's Ellington Field in Houston, Texas in July and September 2022. Flight tracks for all 14 ACCLIP WB-57 research flights from Osan are presented in Figure S1 in Supporting Information S1, and a more detailed summary of individual flight profiles and objectives the available supplement to Pan et al. (2024). For analysis purposes, we categorize the ACCLIP scientific research flights into two groups: ACCLIP-West, where sampling was conducted wholly or partially west of Korea over the Yellow Sea, and ACCLIP-East, where sampling was conducted wholly to the east or the south of Korea. ACCLIP-West data are restricted to a pair of research flights on August 15 and 19, during which outflow from recent deep convection along the Chinese coastline was sampled.

The 2022 ACCLIP campaign builds on a legacy of previous airborne campaigns in the region, such as TRACE-P in 2001 (Blake et al., 2004) and KORUS-AQ in 2016 (Simpson et al., 2020), which sampled OCS at lower altitudes on larger research aircrafts like the NASA DC-8 and P-3B. These earlier campaigns focused on the boundary layer and free troposphere. During KORUS-AQ, pollution plumes in the Yellow Sea region were specifically targeted, revealing extremely high OCS mixing ratios exceeding three times the global mean mixing ratio in the boundary layer, below 2 km (Simpson et al., 2020). By extending measurements for the sample domain into the UTLS, ACCLIP provides critical new data that enhance our understanding of the vertical transport processes and chemical interactions within the ASM system, with considerable implications for the global stratospheric sulfur budget.

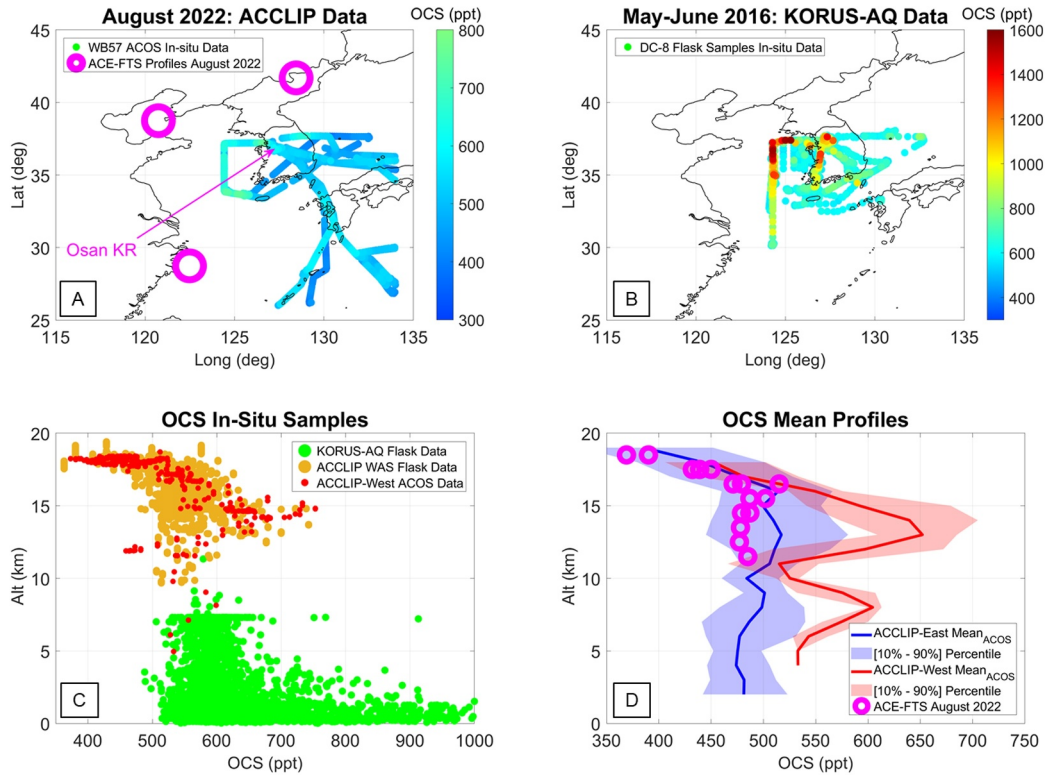

Figure 3. A comparison of OCS measurements from Korea-based airborne sampling campaigns from KORUS-AQ (panel b) and the ACCLIP (panel a). The top panels represent the horizontal sampling domains for both campaigns, while the bottom panels compare vertical profiles. Note the different scales between the top panel color bars. KORUS-AQ (May–June 2016) sampled in the boundary layer and free troposphere-targeting pollution plumes and reported OCS mixing ratios as much 1,600 ppt. OCS measurements during ACCLIP (August 2022) were focused primarily in the upper troposphere and the lower stratosphere, yet the most significant ACCLIP OCS enhancements occur in the ACCLIP-West domain, a similar horizontal spatial domain to the boundary layer enhancements from KORUS-AQ. ACE-FTS profiles sampled in the vicinity of the ACCLIP domain during August 2022 are shown for comparison (panel a, magenta circles).

3.2. In Situ Measurements

During the ACCLIP campaign, OCS samples were collected continuously in flight with the NOAA Airborne Carbonyl Oxides Spectrometer (ACOS), and periodically for offline gas chromatograph analysis with whole air sampler (WAS) stainless steel canisters (Treadaway et al., 2022). This campaign represents the initial deployment of the ACOS instrument, which is similar to the AMICA airborne spectrometer (Kloss et al., 2019) utilizing a modified Los Gatos Research ICOS analyzer (Berkelhammer et al., 2014) with a precision of 100 ppt determined by trace gas calibration with an Airgas certified standard with an analytical uncertainty of 5%. Confirmation of the OCS values during ACCLIP is accomplished by comparison with the WAS canister data, which generally fall within the scope of the ACOS data precision (Figure S3 in Supporting Information S1), particularly the enhancements greater than 600 ppt (see Figure 3c). For the comparison in Figure 3, archived WAS OCS mixing ratios have been reduced by 8% to account for the drift in the comparison standard (E. Atlas, personal communication). The ACCLIP data archive has not yet been updated to reflect these revised values. Anomalously high WAS OCS values in the canister are tentatively attributed to OCS formation within the stainless steel canisters over time (Schuck et al., 2020), and may contribute to higher tropospheric OCS baseline values observed during KORUS-AQ.

For both the ACCLIP and earlier KORUS-AQ campaigns, free tropospheric (2–12 km) OCS values in the region are fairly uniform. The sampling strategy of the WB-57 aircraft during ACCLIP limited sampling in the boundary layer to takeoff and landing. This approach precludes direct comparisons with the most significant enhancements observed during of KORUS-AQ when the vast majority of the sampling occurred in the boundary layer. During ACCLIP, the highest OCS mixing ratios were recorded in the UTLS region (13–16 km) not sampled during

KORUS-AQ. While both ACCLIP-East and ACCLIP-West flights demonstrate elevated OCS levels in the UTLS, the relative abundance of these events in the ACCLIP-West flights suggests a more significant contribution from recent anthropogenic emissions from China. We are confident that the emissions are anthropogenic in origin as the enhanced OCS values correlate with high CO sampled values and short-lived organic chlorine species (Pan et al., 2024), which have primarily anthropogenic sources.

These observations suggest that boundary layer-polluted air parcels in the region can be efficiently lofted via deep convection directly to the UTLS. Comparison of the airborne OCS data with surface measurements is limited by a paucity of active ground sample sites in the region. However, the new AGAGE network site at Gosan, Korea (Jeju Island) did provide consistent OCS in situ measurements using the Medusa GC-MS in the early summer period of 2022 (data Provided via personal communication with the AGAGE Gosan PI Dr. Sunyoung Park) preceding the ACCLIP campaign. The AGAGE Gosan site is ideally situated for studying Chinese anthropogenic emissions transported across the Yellow Sea (Park et al., 2021, 2023), and Geum et al. have developed a technique to separate baseline and emission air parcels utilizing methane abundance (Geum et al., 2024). The Gosan AGAGE early summer baseline OCS mode is consistent with earlier Beijing sampling from 2011 to 2013 (Cheng et al., 2015) of ∼550 ppt (Figure 4). Similarly, the maximum OCS values (>1,000 ppt) reported by Cheng et al. are of similar magnitude to those observed during KORUS-AQ in 2016, and with earlier Beijing measurements from 2001 (Yujing et al., 2002). The lack of observed OCS exceedances of this magnitude during 2022 sampling from either the Gosan surface site or the ACCLIP airborne measurements suggest recent declines in anthropogenic OCS emissions, which is consistent with the overall NOAA GML trend shown in Figure 2c.

The early summer 2022 Gosan OCS measurements and ACCLIP in situ data indicate a correlation between the 550-ppt mode (see dashed line in Figure 4) of the ACCLIP-East distribution and the Gosan baseline data (Figures 4b and 4c). This consistent mode suggests a persistent regional baseline, with the observed mode (∼550 ppt) significantly exceeding the global midlatitude NOAA GML network global average (∼470 ppt) for the sample period (see Figure 2). The Gosan site-measured "pollution" plumes are also of similar magnitude of enhancement to the ACCLIP-West samples (>700 ppt), supporting the hypothesis of minimal dilution of the anthropogenic emission parcels during convective lifting. Convective lifting is the most plausible vertical transport pathway for rapid (compared with dilution timescale) transport of the boundary layer to ∼15 km in the absence of significant topographical features.

4. UTLS Transport

4.1. Deep Convective Transport

It is plausible that convective lifting facilitates the rapid vertical transport of boundary layer air parcels with enhanced OCS concentrations, with minimal dilution, potentially explaining the observed similarities between the ACCLIP UTLS and AGAGE Gosan boundary layer OCS distributions (Figure 4). To affirm this hypothesis, we performed 24-hr three-dimensional backward trajectory analysis using HYSPLIT v5.2.1 with NCEP reanalysis winds for model vertical velocity. For this analysis, individual trajectories originate from the positions along the ACCLIP-West August 19 research flight where significant pollution (CO > 150 ppb) was observed in the UTLS (WB57 sample altitude >12 km). In this case study, we compare these trajectories (Figure 5, pink lines) with two measures of deep convection: cloud top temperature from the Global Precipitation Measurement (GPM) Mission MergeIR product, in the same manner as Pan et al. (2024), and the WMO mean updraft mass flux (MUMF) value at the ERA5 model level 74 (geopotential height ∼12 km). It is evident that the air parcel trajectories from WB-57 sampling locations pass directly through a region of deep convection near the Bohai Sea, which is indicated in both deep convection products (Figure 5). It is therefore likely that significant anthropogenic emissions from the China were transported to the WB-57 sample locations in less than one day.

A similar analysis of the convective influence for all ACCLIP research flights (W. Smith et al., 2023) allows for a statistical analysis of locations where all sampled air parcels most recently encountered a deep convective cloud, using a CloudSat satellite-derived convective cloud top altitude product (Pfister et al., 2022). More details on the methodology and associated uncertainties of the convective influence trajectory analysis—including comparisons of results using different wind reanalysis products and an explanation of the spatial distribution of parcel origin locations relative to the aircraft sampling position—are provided by W. P. Smith et al. (2025). Applying the ACCLIP OCS in situ data to this convective influence product, it is clear that the majority of strong OCS enhancements were sampled in deep convective outflow from the Chinese coastal region (Figure 6c), where the

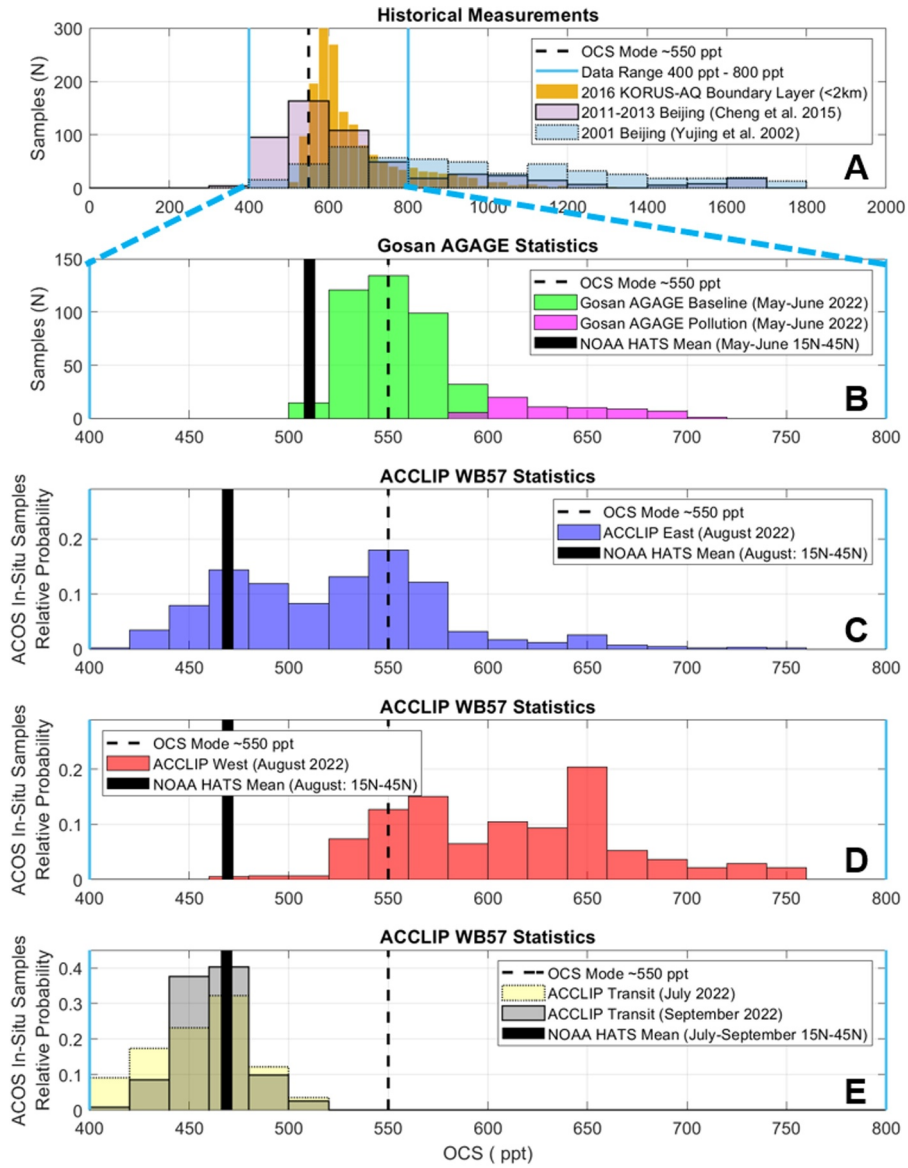

Figure 4. A comparison of OCS sampling near Korea, with a dashed vertical line in all panels at 550 ppt to guide the eye. Panel (a) shows published historical OCS boundary layer measurements in the region during the periods of 2001 (derived from Figure 6 (Yujing et al., 2002)), 2011–2013 (derived from Figure 1 (Cheng et al., 2015)), and 2016 (KORUS-AQ). Panel (b) shows sampling statistics from the GOSAN Advanced Global Atmospheric Gases Experiment (AGAGE) site on Jeju Island, Korea in the early summer period of 2022, segregated into enhanced pollution with origins primarily from China and regional baseline parcels according to the Geum et al., 2024 methane abundance criteria. Panels (c) and (d) show the statistics from the ACCLIP in situ measurements, separated into eastern and western flights, while the bottom panel (e) shows the airborne in situ measurements from the trans-Pacific transit flights between Houston and Korea. For aircraft data, we limit consideration of OCS data to below 380 K (the approximate tropical tropopause) as to not introduce bias from older stratospheric air parcels, which may be OCS-depleted. The NOAA Global Monitoring Laboratory mean from midlatitude sites (15–45 N) for the relevant period is also overlaid in each panel in solid black. The AGAGE-observed maximum OCS mixing ratios occur in "polluted plumes" (defined by high methane abundance), and the magnitude of these enhancements agree well with ACCLIP Western sampled events. Note the difference in *x*-axis scale between Panel (a) and Panels (b–e).

most significant anthropogenic emissions are estimated (Figure S5 in Supporting Information S1). This region is colocated with strong enhancements in carbon monoxide (CO) abundance (Figure 6d). Given the shorter atmospheric lifetime for CO of less than 40 days in the summertime free troposphere in ACCLIP sample domain (Duncan et al., 2007), the observed enhancements suggests the influence of recent anthropogenic emissions.

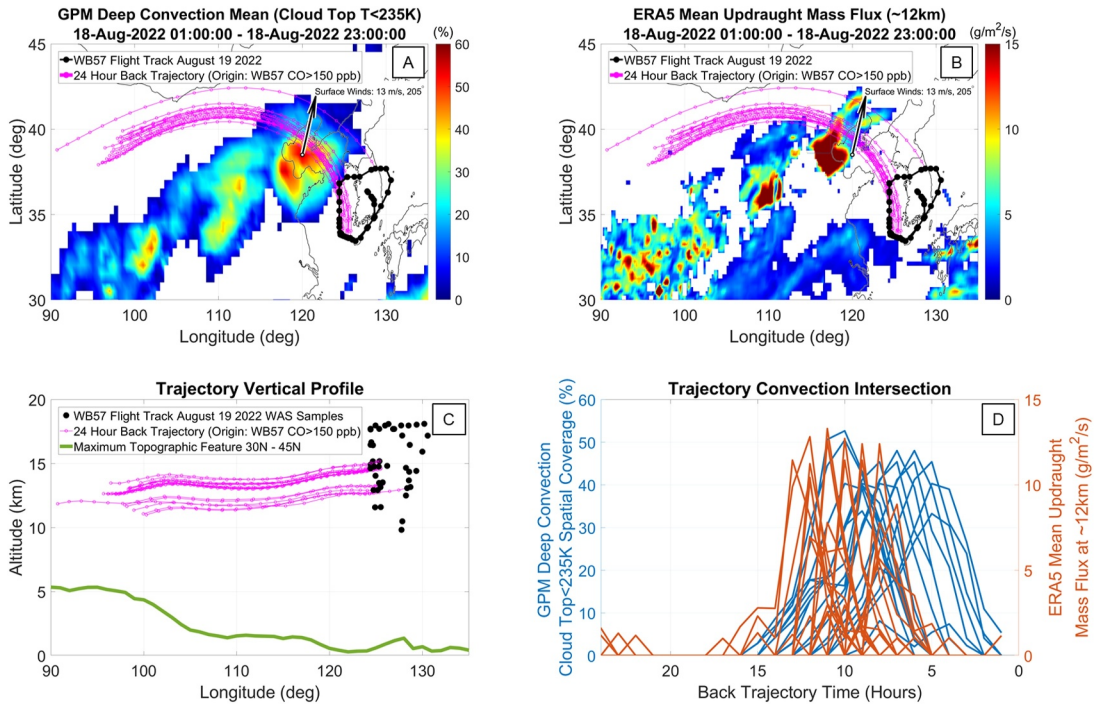

Figure 5. Analysis of the ACCLIP OCS source regions via back trajectory analysis. These plots represent case studies from the 19 August 2022 ACCLIP flight where 24-hr back trajectories (pink lines) are launched from locations along the flight track where extreme carbon monoxide abundances were reported (>150 ppb) in the Upper Troposphere and Lower Stratosphere (UTLS). These trajectories are overplotted on 24-hr average measures of deep convection, GPM MergeIR cold ($T < 235$ K) cloud top abundance, and percentage cloud cover during August 19th (panel (a)) and the WMO forecast mean updraft mass flux at model level 74 and geopotential height ~ 12 km (panel (b)). For both measures, back trajectories from the flight track pass through deep convection in the vicinity of the Chinese Bohai Sea coastline. NCEP surface level winds near the region of maximum convective lifting in the middle of the Bohai Sea (black arrow with origin 38.5 N, 120E) on 8/18 18:00 UTC are flowing northeasterly, opposite the UTLS winds which follow the ASM circulation southeast toward the ACCLIP sample domain. The different parameterizations (panels (a) and (b)) result in temporal inconsistencies of several hours in the timing of the backward trajectories intersecting the strongest convective regions (panels (c) and (d)), underscoring the uncertainties in accurately identifying precise anthropogenic source regions.

Mean OCS mixing ratios originating from convective influence further inland remain somewhat elevated in line with the Gosan AGAGE baseline parcels (~75 ppt above NOAA GML data midlatitude seasonal mean).

Morrison et al. demonstrated that the convective mass flux parameterization is sensitive to horizontal grid spacing (Morrison et al., 2015), and the convective parameterizations we consider here utilize a variety of spatial scales. The GPM satellite product utilizes fine spatial (4 km) and temporal resolution (30 min) observations but is an indirect measure of convection estimated from cloud top temperature. The CloudSat convective cloud top product uses a different spatial resolution (0.25°), with a 3-hr temporal resolution. The WMO MUMF product utilized in ERA5 mass flux is a twice daily hourly forecast of mass flux, also with 0.25-degree resolution. Convective mass fluxes are provided by the ECMWF Integrated Forecasting System model with its changed cloud convection parameterization scheme (Hersbach et al., 2020) originally based on Tiedtke (1989). The spatial discrepancies in Figure 5 maybe attributed to the spatial and temporal differences between the GPM and MUMF parameterizations. While the difference between the forecast mass flux and the observed deep convective cloud tops in the case study is minor, smaller and short-lived convective features like cumulus congestus turrets may be critical for correctly accounting for OCS flux to the UTLS.

4.2. ASM Entrainment

Using the same HYSPLIT modeling technique to produce 30-days forward trajectories from the upper troposphere ACCLIP-East samples indicates transport around the perimeter of the ASM (defined by ERA5 dynamic tropopause height (Hoffmann & Spang, 2022)), while conversely ACCLIP-West parcels with the highest OCS abundance tend to become entrained into the core of the anticyclone (Figure 7). These results suggest that the most significant OCS enhancements measured during the ACCLIP-West flights will predominantly become confined in the core of the ASM, while ACCLIP-East samples tend to flow around the southern edge of the ASM and are

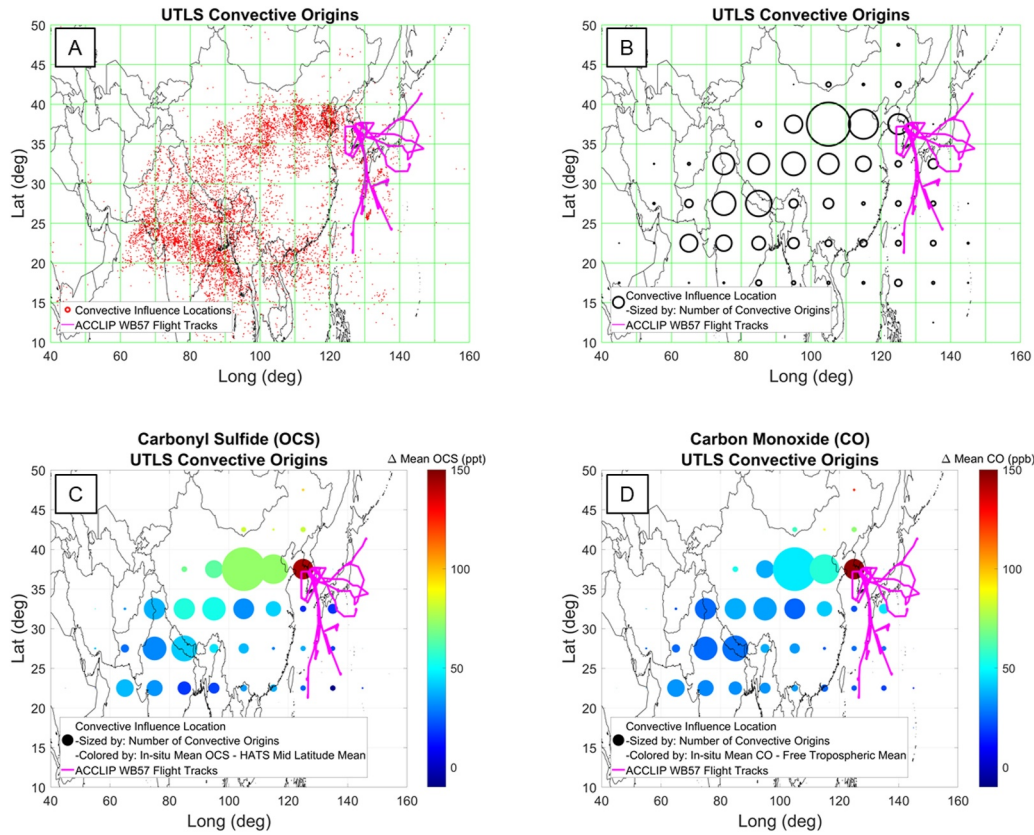

Figure 6. The spatial distribution of deep convective influence locations for all WB-57 ACCLIP research flight upper tropospheric samples (flight tracks shown in magenta) combined with in situ mixing ratios from Airborne Carbonyl Oxides Spectrometer data. ACCLIP convective influence locations from the W. Smith et al., 2023 data set (panel (a)) are gridded into 10° × 5° bins (panel (b)) to represent the frequency of different regions scaled by marker diameters (See Figure S4 in Supporting Information S1 for higher frequency gridding of the data set). In the bottom panels, the panel (b) markers are colored to indicate the mean in situ trace gas mixing ratio anomaly. Panel (c) represents the mean OCS value in each grid box with the NOAA Global Monitoring Laboratory August midlatitude (15–45 N) mean subtracted, and the Panel (d) represents the mean CO value in each grid box with an approximate mean free tropospheric baseline (40 ppb) subtracted. An air parcel age may be inferred from the difference in atmospheric lifetime between these molecules. The highest abundances for both species occur in the vicinity of the Bohai Sea, presumably a result of anthropogenic emissions rapidly lofted via deep convection. Anthropogenic sourcing is supported by the relative abundance of CO in the measurements from this region.

transported westward. These transport statistics highlight the importance of transient deep convective lifting to populate the core of the ASM anticyclone with enriched OCS parcels.

Similar OCS enhancements in the UTLS within the ASM boundary have been previously noted from satellite observations, specifically the ACE-FTS data set (Park et al., 2008). While these remote retrievals provided valuable insights into OCS behavior in this region, the analysis has been limited by poor sampling statistics of remote sensing platforms (see Section 5), and a lack of in situ validation. A gap in coordinated measurements has left uncertainties in the accuracy and interpretation of the satellite data. This highlights the need for data sets like ACCLIP that incorporate in situ measurements to corroborate and refine these observations to quantify the UTLS OCS abundance available for stratospheric transport though the ASM.

5. Comparison With UTLS Trends

While in situ sampling data sets remain extremely limited, OCS measurements from the wide-ranging Atmospheric Tomography Mission (AToM) and HIAPER Pole-to-Pole Observations (HIPPO) aircraft campaigns (2009–2018) have previously been used to validate OCS distribution in global models. This analysis has demonstrated that models underestimate free tropospheric OCS concentrations in the Northern Hemisphere western Pacific (Ma et al., 2021). The discrepancy may be attributed in part to underestimates of both direct and

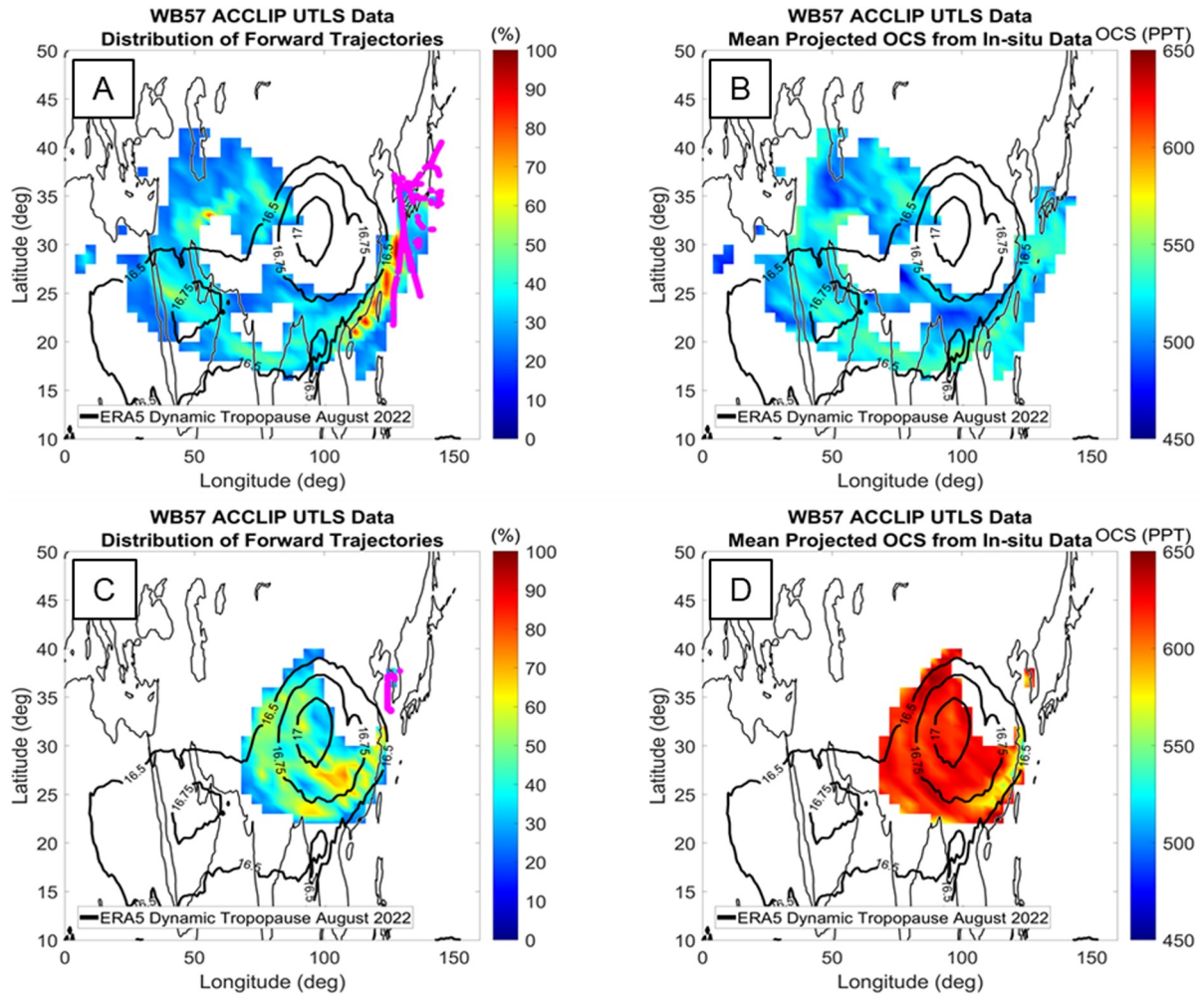

Figure 7. Statistical distributions of 30-day forward trajectories from ACCLIP in situ sample locations (HYSPLIT 5.2.1 with NCEP reanalysis winds). The left panels show spatial distributions of forward trajectories launched from the flight path in the Upper Troposphere and the Lower Stratosphere (350–370 K) for ACCLIP-East sampling (top) and ACCLIP-West sampling (bottom). Flight tracks shown in magenta. The right panels project the ACCLIP in situ OCS values along the forward trajectories with no dilution. The August 2022 dynamic tropopause height contours are overlaid on all panels to indicate the region of the ASM anticyclone during the ACCLIP campaign.

precursor (primarily CS_2) anthropogenic emissions from Asia (Zumkehr et al., 2018). Significant OCS precursor vertical transport is supported by some observations of extremely high CS_2 concentrations (>50 ppt) in the free troposphere by the NCAR Trace Organic Gas Analyzer instrument (Apel et al., 2015) on the GV aircraft during the ACCLIP campaign (Honomichl, 2023); see Pan et al. (2024) for a discussion of the GV flights. The ACCLIP measurements therefore provide further evidence for a regional enhancement of anthropogenic emission transport from Asia in the upper troposphere. In this section, we compare the ACCLIP in situ ACOS OCS data set with trends reported by remote sensing retrievals in the UTLS and examine how these features are represented by global models.

5.1. Remote Sensing Data Sets

The NDACC network uses ground-based Fourier transform infrared (FTIR) spectrometry to monitor atmospheric trace gases, including OCS, at sites distributed across the globe (De Mazière et al., 2018). In the northern midlatitude regime relevant for ACCLIP measurements, OCS vertical profiles are retrieved with commercial Bruker spectrometers at four sites (Figure 8a). A western Pacific midsummer enhancement trend in OCS values is evident in the NDACC archive data, with the highest midlatitude OCS free tropospheric mixing ratios reported at the Japanese Tsukuba site. The mean UTLS enhancement is somewhat smaller than that observed during ACCLIP

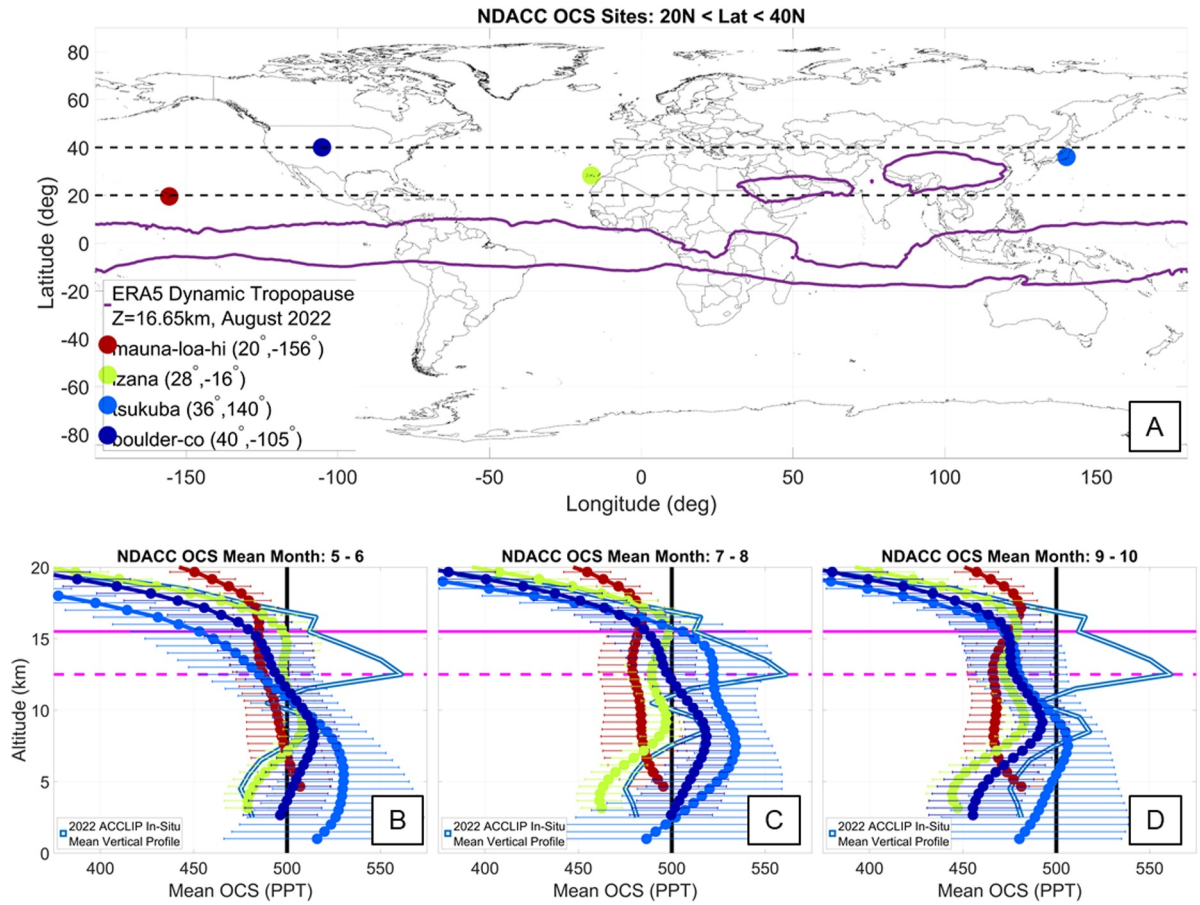

Figure 8. Network for the Detection of Atmospheric Composition Change-archived mean vertical OCS profiles, with standard deviations, from ground-based FTIR measurements in the northern midlatitudes (20–40 N) at Mauna Loa, HI, USA, Izana, Spain, Tsukuba, Japan and Boulder, CO, USA. Profiles are averaged for the entire archive of each site, from left to right early summer (May–June, panel (b), middle summer (July–August, panel (c) and late summer (September–October, panel (d)), overlaid with the mean Airborne Carbonyl Oxides Spectrometer OCS vertical profile from the ACCLIP campaign science flights. In the top panel, the August 2022 ERA5 dynamic tropopause 16.65-km contour is shown as a purple line. In the bottom panels, the horizontal black line represents the approximate global surface mean OCS mixing ratio (∼500 ppt), and the vertical pink lines indicate approximate levels above (15.5 km) and below (12.5 km) the tropical tropopause (Fueglistaler et al., 2009).

(Figure 8c), likely a result of the site's location outside the core of the ASM. The UTLS OCS enhancement in the NDACC Japan site maybe attributed in part to eastward extension of the ASM anticyclone, which transports Asian anthropogenic emissions into the western Pacific (Pan et al., 2022).

The ACE-FTS satellite began operation in 2004 and is currently the only vertically resolved OCS satellite measurement platform with global coverage (Boone et al., 2023), after the decommissioning of complimentary satellite platforms MIPAS (2002–2012) (Glatthor et al., 2017) and TES (2004–2018) (Kuai et al., 2014). ACE-FTS has relatively sparse profiling in the equatorial and midlatitude regions, particularly during the summer season (Figure 9, left panels). Therefore, significant temporal averaging is required to achieve reasonable sampling statistics. Despite these limitations, the ACE-FTS data set has been used to demonstrate a recent change in the global upper tropospheric (8.5–10.5 km) OCS abundance of −4.53 ppt/year (Schmidt et al., 2024), which correlates with the stratospheric trend reported from the NDACC network, which shows negative stratospheric trends for stations at low latitudes (Hannigan et al., 2022).

Enhanced abundance of OCS in the UTLS above level of zero radiative heating (LZRH) are the most significant for stratospheric transport. Air parcels above this level can slowly ascend into the stratosphere as a result of diabatic heating during the prolonged anticyclone period. This process is efficient for OCS as its upper tropospheric lifetime (>1 year) exceeds the approximately 1-month diabatic heating transport time to reach the 380-K tropopause threshold with 1–1.5 K/day heating (Vogel et al., 2019). To estimate the magnitude of this transport

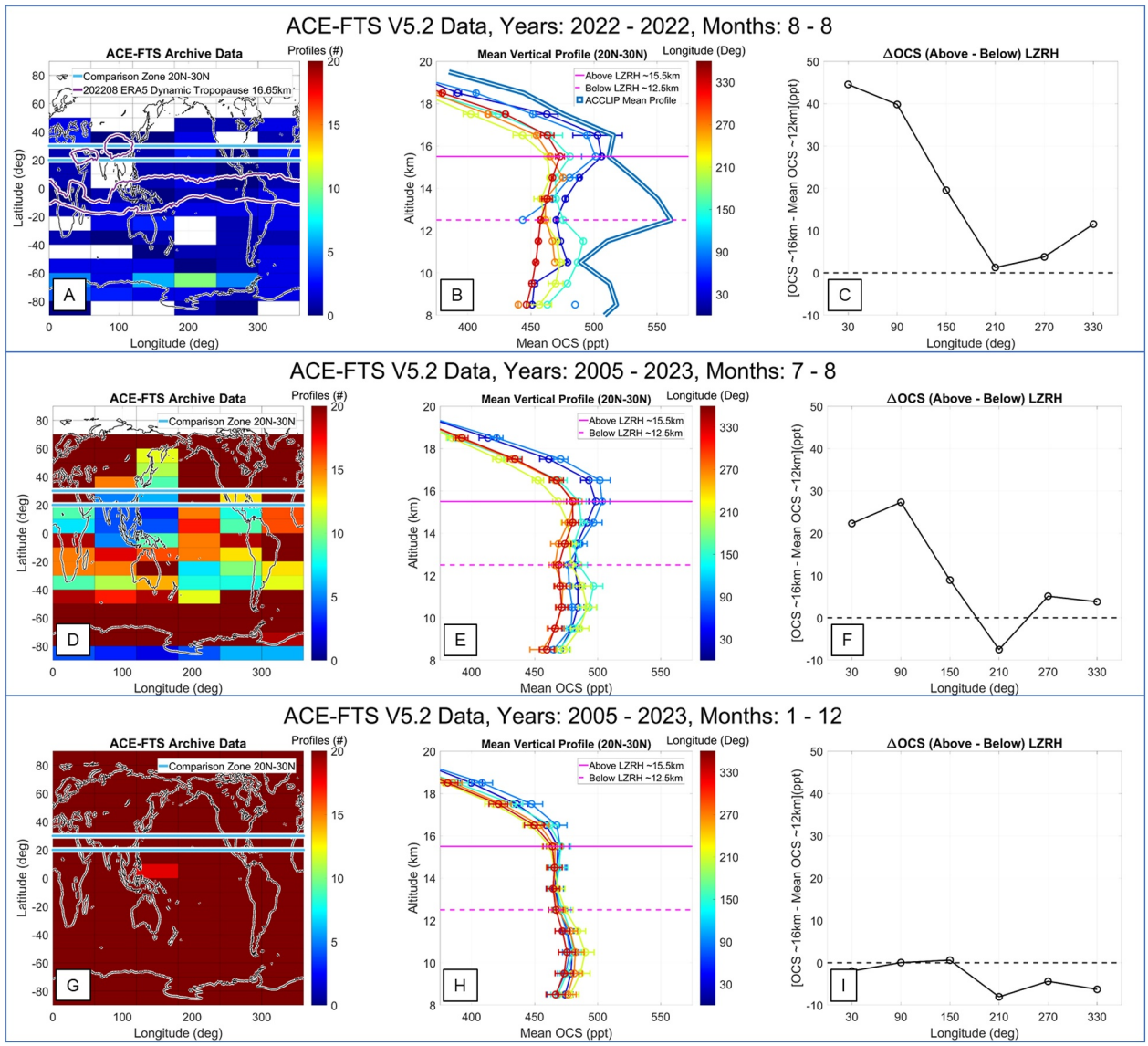

Figure 9. Analysis of satellite-derived OCS vertical distributions using the ACE-FTS v5.2 data set in several periods: 1. during the ACCLIP campaign August 2022, with the Airborne Carbonyl Oxides Spectrometer ACCLIP mean profile overlaid as in Figure 8 (top panels); 2. the middle summer season for the entire ACE-FTS archive (middle panels); and 3. the entire ACE-FTS V5.2 data set (bottom panels). Sampling statistics during these intervals are shown in the left column where colors represent the number of profiles in that grid box. Mean vertical profiles along the northern edge tropical tropopause layer (20–30 N, cyan lines left column) are shown in the middle column. The right panels show a longitudinal comparison OCS mixing ratio above the LZRH (15.5 km) with the mean zonal mixing ratio below the LZRH (12.5 km). Note that the purple contours in the top left panel represent the tropopause heights from Figure 8 to visualize the extent of the August 2022 ASM boundaries.

pathway, we will compare OCS mixing ratios above (15.5 km) and below (12.5 km) the tropical tropopause layer (TTL) level of zero radiative heating (Fueglistaler et al., 2009). Although various measures of atmospheric depth might be more pertinent for characterizing changes in the LZRH within the TTL, including potential temperature, we have chosen to use a straightforward altitude-based definition to facilitate comparison with the vertical retrieval parameters from the FTIR remote sensing platforms. Although the TTL region is extended northward due to the ASM, our comparison will focus on longitudinal averages at the northern edge of the TTL region (20–30N) to provide consistency across all longitudinal bands.

The northern edge of the tropics and the ASM region specifically were poorly sampled by ACE-FTS during the ACCLIP campaign period of August 2022 with less than 10 profiles within the eastern ASM boundary. We therefore consider mean profiles over a wide spatial domain, 10-degree latitude by 60-degree longitude, to ensure at least one vertical profile is available for comparison over the entire globe in the 20–30 N band (Figure 9a). The

limited remote sensing opportunities within the ASM domain by both the ACE-FTS satellite (poor sampling statistics) and the NDACC network (outside ASM boundary) highlight the importance of the ACCLIP campaign in situ UTLS measurements for characterization of ASM transport.

During the August 2022 ACCLIP sampling period, averaging of the available ACE-FTS profiles indicates a maximum UTLS enhancement of 45 ppt between 15.5 km longitudinal mean values and the global mean at the 12.5 km level (Figure 9c). Above the LZRH level (15.5 km), there is reasonable agreement between the OCS magnitude of the ACE-FTS profiles in the ASM region and the mean ACCLIP vertical profile. However, there is a notable discrepancy between the satellite profiles and in situ data lower in the UTLS. The ACCLIP trace gas enhancements near 13 km are likely due to detrainment from convective lifting events, where parcels lifted to the upper troposphere yet below the LZRH, will rapidly descend. Limited satellite profiles in the ASM domain therefore hamper characterization of this transient convective lifting mechanism. However, a general agreement of the satellite and ACCLIP in situ data at high altitudes supports the efficacy of ACE-FTS trends to consider the slower diabatic heating mechanism for parcels injected above the LZRH.

Using midsummer (July–August) mean data from the all full sampling years of the ACE-FTS V5.2 archive (2005–2023), a persistent enhancement in the OCS vertical profile in the UTLS is apparent across most longitudinal ranges, peaking at approximately 90° longitude in the ASM core region (Figure 9e). The mean summer UTLS enhancement above the LZRH in the ASM region is 27 ppt from the full archive data set (Figure 9e). This UTLS enhancement in the OCS mixing ratio disappears when considering an annual mean (Figure 9h). Though these OCS transport trends are derived from sparse satellite data, they represent the only ongoing long-term observations available in the UTLS for comparison with global chemical models.

5.2. Model Considerations of Vertical Transport

Lagrangian models have been used to demonstrate that the ASM is an effective pathway for transport of long-lived chemical tracers into the tropical pipe (Randel et al., 2010). Recent analysis confirms that this pathway has an approximately 30% transportation efficiency from the ASM to the stratosphere for air parcels lifted via deep convection above a potential temperature threshold of 350 K (X. Yan et al., 2019). Considering another long-lived tracer species, HCN, Ploeger et al. (2017) showed via model and satellite observations that as much as 5% of the tropical pipe air mass results from ASM transport after 9–10 months for a 2010–2013 climatology. These modeling studies support a direct pathway for enhanced Asian OCS emissions to be transported to the stratosphere via deep convective lifting in the ASM.

Chemistry-climate models (CCMs) have been shown to well represent transport of many trace gas species compared with previous airborne campaigns in the ASM region (W. P. Smith et al., 2024). However, CCMs significantly underestimate the magnitude of OCS observed in the ASM UTLS compared to ACE-FTS trends (Figure 10, right panels). When considering the atmospheric sulfur budget, models like CESM2 are typically run with a fixed global surface OCS boundary condition (Figure 2, green line), which results in a homogenous tropospheric OCS distribution, precluding any UTLS enhancement compared to the surface mean mixing ratio (Figure 10, top panels). Despite this limitation, Sheng et al. have demonstrated that global models with fixed OCS boundaries can replicate historical stratospheric aerosol data with reasonable accuracy (Sheng et al., 2015). However, there remains some uncertainty for this validation based on the anomalously large mixing ratios of SO_2 in the UTLS compared with recent airborne observations (Rollins et al., 2017). Incomplete representation of temporal trends of OCS abdunances, both multiyear (Hannigan et al., 2022; Schmidt et al., 2024) and seasonal (Montzka et al., 2007), also add uncertainty to model analysis when fixed boundary values are used (Figure 2).

A recent Toulouse Offline Model of Chemistry and Transport (TOMCAT) 3-D climate transport model study demonstrated that modeled OCS in the stratospheric photolysis region (>25 km in the tropics) is underestimated compared to ACE-FTS satellite observations by as much as 75 ppt over the period of 2004–2018 (Cartwright et al., 2023). A discrepancy in OCS of this magnitude would result in a significant underestimate in the sulfur available for particle formation and growth (1 ppt OCS can produce in excess of 3 ng S/kg sulfate aerosol depending on density from water uptake), which has implications for global radiative forcing from particles formed in the Junge layer. The estimated 75 ppt OCS model deficit in the middle stratosphere would result in a 10% inconsistency in the sulfate aerosol concentration (~225 ng/kg), which unfortunately lies within the uncertainty bounds of satellite aerosol retrieval products at these altitudes (Taha et al., 2021). While some of these

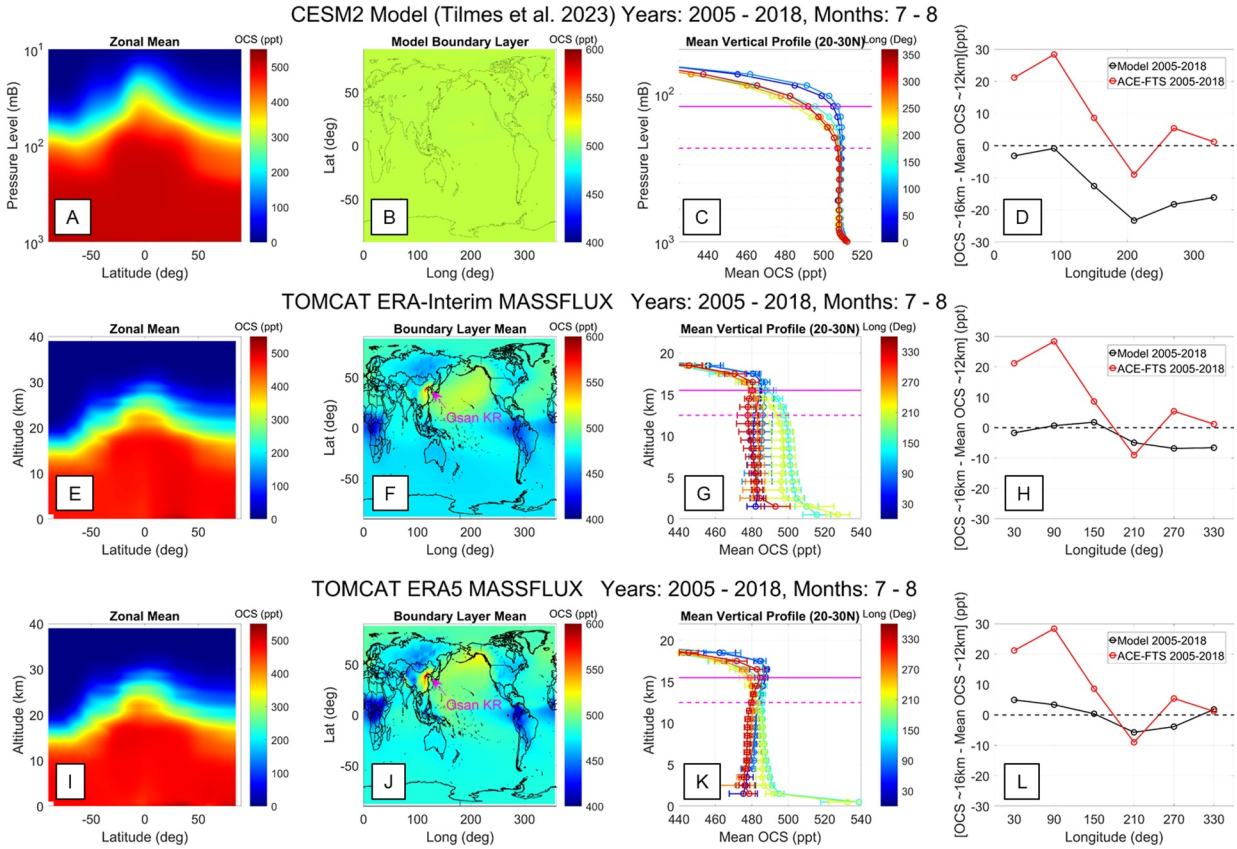

Figure 10. A comparison of the modeled mean OCS enhancement in the Upper Troposphere and Lower Stratosphere (UTLS) during the midsummer period (July–August) for 2005–2018. Model runs with a fixed OCS boundary layer like this CESM2 model (top panels) are unable to reproduce the ASM-driven OCS enhancement in the UTLS (Tilmes et al., 2023). Models which include surface emissions, particularly anthropogenic emissions, like the TOMCAT model (middle and bottom panels) do reproduce the seasonal OCS enhancement in the UTLS (Cartwright et al., 2023) with a lower magnitude than observed by ACE-FTS. The modeled convective mass fluxes play a significant role in representing this feature, with ERA5 mass fluxes (bottom panels) showing better, though still poor, agreement with the ACE-FTS data than the ERA-Interim flux parameterization (middle panels).

underestimations may result from imperfect photolysis parameterization, a portion of the sulfur budget deficit may also arise from models' inability to accurately represent vertical ASM transport of OCS into the stratosphere.

To explore the representation of the ASM UTLS enhancement, we consider several simulations of the TOMCAT 3D model that include best estimates of global OCS sources and sinks (including anthropogenic emissions). The TOMCAT run, which uses the ERA-Interim convective mass flux fluxes (Cartwright et al., 2023), does show a slight UTLS enrichment in the ASM region (Figure 10, middle row) in the summer months (July–August). TOMCAT is rerun using the same parametrization scheme, but the newer ERA5 reanalysis, and the ASM-UTLS OCS abundance is further enhanced (Figure 10, bottom panels). This difference is expected as ERA5 has stronger vertical transport than ERA-Interim (Li et al., 2020). Nevertheless, the ERA5 mass flux-driven model still significantly underestimates the ASM UTLS OCS enhancement compared to ACE-FTS (Figure 10 right panels). The inability to replicate satellite-observed OCS trends in the UTLS may result from an underestimation of extreme convective vertical transport events (Hoffmann et al., 2023).

6. Discussion

The ACCLIP high-altitude aircraft data set offers some of the first in situ confirmation of efficient deep convective transport for anthropogenic OCS emissions in the ASM region, previously reported by remote sensing platforms. UTLS measurements indicate a similar magnitude of regional baseline and pollution enhancements as the boundary-layer concentrations were observed at a local AGAGE ground site, suggesting vertical transport on short timescales with minimal dilution. Trajectory analysis indicates that parcels enriched in OCS primarily

originate from deep convection around northern China and may then become preferentially entrained in the core of the ASM. A lack of vertical profiles near the core of the anticyclone limits the ability to use the ACCLIP data set to constrain tropopause fluxes, so this work serves to highlight the potential efficacy of the ASM vertical transport mechanism's role in the stratospheric sulfur budget.

Previous Lagrangian transport studies have demonstrated that a subset of ASM-entrained parcels injected above the LZRH may be transported into the peak stratospheric OCS photolysis region (tropical pipe) in under a year. With the total ASM contribution to the tropical pipe population estimated at ∼5%, the most generous estimate of the middle stratospheric OCS mixing ratio enhancement from ASM transport would be at most 12.5 ppt based on the preferential transport of the most polluted UTLS parcels (750 ppt) sampled during ACCLIP. By contrast, Cartwright et al. (2023) model-satellite comparison study indicated that current models may underestimate the OCS burden in the middle stratosphere by as much as 75 ppt. This discrepancy suggests that the underrepresented ASM vertical transport may only partially explain the model OCS deficit in the tropical pipe, with additional uncertainties in OCS photolysis parameterization and stratospheric dynamical transport also likely contributing.

Here, we have demonstrated that CCM models significantly underestimate the magnitude of the ASM vertical transport mechanism. Inclusion of regional anthropogenic emissions improves model skill in replicating satellite observed trends, yet outstanding uncertainties in both OCS emissions inventories and convective parameterizations remain significant limitations to model efficacy. The importance of the ASM transport mechanism for the stratospheric sulfur budget may be further enhanced if rising sea surface temperatures increase the frequency of deep convective mass flux in a warming climate (Cheng et al., 2022). Upcoming continuous measurements in the region, including the new NDACC site in Hefei, China (Wang et al., 2017), along with enhanced reanalysis data sets and higher precision global models may help to reduce the uncertainty associated with both emissions inventories and convective parameterizations.

The observed ACCLIP UTLS enhancements highlight the limitations of the homogenous tropospheric OCS assumption. Due to sparse vertical OCS data in the equatorial region, quantifying the impact of the transient sulfur transport on stratospheric aerosol formation remains challenging. Additional in situ aircraft and balloon data for the primary sulfate aerosol precursors (OCS and SO_2) are therefore essential for improving our understanding, and model validation of the upper atmospheric sulfur budget. Understanding the crucial role of OCS in the stratosphere is particularly important given the increasing potential for SAI as a climate mitigation strategy.

7. Conclusion

The 2022 ACCLIP field campaign delivered unprecedented in situ observations of OCS in the UTLS region of Northern Asia. These measurements revealed peak OCS enhancements exceeding the global baseline (∼500 ppt) by 50%, which are likely attributed to transport of anthropogenic emissions from China. A strong correlation between regional surface and airborne data validates the ACCLIP in situ data set and underscores the effectiveness of convective lifting for vertical transport of enriched OCS parcels to the UTLS during the midsummer season. Despite the significant OCS enhancements observed during ACCLIP, comparisons to extreme values observed during previous campaigns in the region support a declining trend in OCS and precursor anthropogenic emissions.

This study underscores the significant impact of anthropogenic emissions from Asia on the UTLS OCS abundance, particularly during the midsummer months when intermittent deep convection facilitates efficient vertical transport. Trajectory analysis originating from convective sources indicates that the OCS enhancements observed during ACCLIP result from deep convective lifting in China. Colocated enhancements in CO mixing ratios support anthropogenic sourcing of these UTLS parcels. Despite this confirmation, precise sourcing of emission sites is limited by a paucity of surface OCS sampling throughout the region. The majority of the enriched OCS parcels will travel to the core of the ASM allowing for efficient transport above the tropopause, impacting the stratospheric sulfur budget.

Our comparison with limited satellite retrievals confirms the persistence of the midsummer-enhanced OCS trend in the UTLS. However, current models underestimate this feature, and the discrepancy maybe partially a result of an underestimation of the vertical transport of Chinese anthropogenic emissions. These findings highlight the need for a reassessment of global models to better represent regional OCS emissions and improve convective parameterizations, thereby enhancing predictions of stratospheric sulfate aerosol formation and its climate implications.

Data Availability Statement

The data and software presented in this manuscript are publicly available from the following sources:

ACCLIP WB-57 Data set: NASA/LARC/SD/ASDC. (2024).
KORUS-AQ Data set: NASA/LARC/SD/ASDC (2022).
GPM MERGEIR Data set: Janowiak et al. (2017).
WMO MUMF Data set: European Centre for Medium-Range Weather Forecasts (ECMWF). (n.d.).
TOMCAT ERA5 Model Data set: Gurganus (2024).
HYSPLIT Model: Stein (2015).
NCEP Reanalysis: National Centers for Environmental Prediction/National Weather Service/NOAA/U.S. Department of Commerce (1995).
NDACC FTIR Data: Network for the Detection of Atmospheric Composition Change (NDACC). (n.d.).
ACE-FTS V5.2 Retrievals: SCISAT Team. (n.d.).
NOAA GML OCS Flask Data: Hu et al. (2021).

Acknowledgments
The ACCLIP campaign was supported by NSF, NASA, NOAA, and the Office of Naval Research (ONR). We gratefully acknowledge the invaluable contributions of Steve Ciciora and RuShan Gao in the design and deployment of the ACOS spectrometer during the ACCLIP campaign. We also extend our thanks to Ewa Bednarz, Sean Davis, Simone Tilmes, and Mike Cartwright for their crucial support in analyzing the model data. Special thanks are due to the NOAA GML and Gosan AGAGE teams, particularly to the principal investigators, Steve Montzka and Sunyoung Park, for their assistance with interpreting the ground-based site data. Additionally, we appreciate the significant role played by Victoria Treadaway and Katie Smith in the interpretation of the WB-57 whole air sampler OCS data during ACCLIP. This research was supported by the NOAA cooperative agreement NA22OAR4320151, for the Cooperative Institute for Earth System Research and Data Science (CIESRDS) and the NOAA Earth's Radiation Budget Initiative (#03-01-07-001). Whole air sampler data collection and analysis from the ACCLIP campaign is supported by NASA Grant 80NSSC22K1284 and NSF-AGS Grant 1853948. The TOMCAT modeling was supported by NERC grants NE/V011863/1 and NE/X006328/1. Funding for the Atmospheric Chemistry Experiment (ACE-FTS) is provided by the Canadian Space Agency. The National Center for Atmospheric Research is sponsored by the National Science Foundation. The NCAR FTS observation programs at Boulder, CO and Mauna Loa, HI are supported under contract by the National Aeronautics and Space Administration (NASA). We wish to thank NOAA for support of the MLO site. The NDACC data used in this publication were obtained from Isao Murata (PI, Tsukuba, JP) and James Hannigan (PI MLO, Boulder, CO), and are available through the NDACC website, www.ndacc.org. The statements, findings, conclusions, and recommendations are those of the author(s) and do not necessarily reflect the views of NOAA or the U.S. Department of Commerce.

References

Andrews, A. E., Boering, K. A., Daube, B. C., Wofsy, S. C., Loewenstein, M., Jost, H., et al. (2001). Mean ages of stratospheric air derived from in situ observations of CO2, CH4, and N2O. *Journal of Geophysical Research*, *106*(D23), 32295–32314. https://doi.org/10.1029/2001JD000465

Apel, E. C., Hornbrook, R. S., Hills, A. J., Blake, N. J., Barth, M. C., Weinheimer, A., et al. (2015). Upper tropospheric ozone production from lightning NO-impacted convection: Smoke ingestion case study from the DC3 campaign. *Journal of Geophysical Research: Atmospheres*, *120*(6), 2505–2523. https://doi.org/10.1002/2014JD022121

Belviso, S., Remaud, M., Abadie, C., Maignan, F., Ramonet, M., & Peylin, P. (2022). Ongoing decline in the atmospheric COS seasonal cycle amplitude over western Europe: Implications for surface fluxes. *Atmosphere*, *13*(5), 812. https://doi.org/10.3390/atmos13050812

Berkelhammer, M., Asaf, D., Still, C., Montzka, S., Noone, D., Gupta, M., et al. (2014). Constraining surface carbon fluxes using in situ measurements of carbonyl sulfide and carbon dioxide. *Global Biogeochemical Cycles*, *28*(2), 161–179. https://doi.org/10.1002/2013GB004644

Berry, J., Wolf, A., Campbell, J. E., Baker, I., Blake, N., Blake, D., et al. (2013). A coupled model of the global cycles of carbonyl sulfide and CO2: A possible new window on the carbon cycle. *Journal of Geophysical Research: Biogeosciences*, *118*(2), 842–852. https://doi.org/10.1002/jgrg.20068

Blake, N. J., Streets, D. G., Woo, J.-H., Simpson, I. J., Green, J., Meinardi, S., et al. (2004). Carbonyl sulfide and carbon disulfide: Large-scale distributions over the western Pacific and emissions from Asia during TRACE-P. *Journal of Geophysical Research*, *109*(D15). https://doi.org/10.1029/2003JD004259

Boone, C. D., Bernath, P. F., & Lecours, M. (2023). Version 5 retrievals for ACE-FTS and ACE-imagers. *Journal of Quantitative Spectroscopy and Radiative Transfer*, *310*, 108749. https://doi.org/10.1016/j.jqsrt.2023.108749

Brühl, C., Lelieveld, J., Crutzen, P. J., & Tost, H. (2012). The role of carbonyl sulphide as a source of stratospheric sulphate aerosol and its impact on climate. *Atmospheric Chemistry and Physics*, *12*(3), 1239–1253. https://doi.org/10.5194/acp-12-1239-2012

Campbell, J. E., Whelan, M. E., Seibt, U., Smith, S. J., Berry, J. A., & Hilton, T. W. (2015). Atmospheric carbonyl sulfide sources from anthropogenic activity: Implications for carbon cycle constraints. *Geophysical Research Letters*, *42*(8), 3004–3010. https://doi.org/10.1002/2015GL063445

Cartwright, M. P., Pope, R. J., Harrison, J. J., Chipperfield, M. P., Wilson, C., Feng, W., et al. (2023). Constraining the budget of atmospheric carbonyl sulfide using a 3-D chemical transport model. *Atmospheric Chemistry and Physics*, *23*(17), 10035–10056. https://doi.org/10.5194/acp-23-10035-2023

Cheng, K.-Y., Harris, L., Bretherton, C., Merlis, T. M., Bolot, M., Zhou, L., et al. (2022). Impact of warmer sea surface temperature on the global pattern of intense convection: Insights from a global storm resolving model. *Geophysical Research Letters*, *49*(16), e2022GL099796. https://doi.org/10.1029/2022GL099796

Cheng, Y., Zhang, C., Zhang, Y., Zhang, H., Sun, X., & Mu, Y. (2015). Characteristics and anthropogenic sources of carbonyl sulfide in Beijing. *Journal of Environmental Sciences*, *28*, 163–170. https://doi.org/10.1016/j.jes.2014.05.052

Crutzen, P. J. (1976). The possible importance of CSO for the sulfate layer of the stratosphere. *Geophysical Research Letters*, *3*(2), 73–76. https://doi.org/10.1029/GL003i002p00073

Danabasoglu, G., Lamarque, J.-F., Bacmeister, J., Bailey, D. A., DuVivier, A. K., Edwards, J., et al. (2020). The Community Earth System Model Version 2 (CESM2). *Journal of Advances in Modeling Earth Systems*, *12*(2), e2019MS001916. https://doi.org/10.1029/2019MS001916

Davis, N. A., Visioni, D., Garcia, R. R., Kinnison, D. E., Marsh, D. R., Mills, M., et al. (2023). Climate, variability, and climate sensitivity of "middle atmosphere" chemistry configurations of the community Earth system model version 2, whole atmosphere community climate model version 6 (CESM2(WACCM6)). *Journal of Advances in Modeling Earth Systems*, *15*(9), e2022MS003579. https://doi.org/10.1029/2022MS003579

De Mazière, M., Thompson, A. M., Kurylo, M. J., Wild, J. D., Bernhard, G., Blumenstock, T., et al. (2018). The network for the detection of Atmospheric Composition Change (NDACC): History, status and perspectives. *Atmospheric Chemistry and Physics*, *18*(7), 4935–4964. https://doi.org/10.5194/acp-18-4935-2018

Duncan, B. N., Logan, J. A., Bey, I., Megretskaia, I. A., Yantosca, R. M., Novelli, P. C., et al. (2007). Global budget of CO, 1988–1997: Source estimates and validation with a global model. *Journal of Geophysical Research*, *112*(D22). https://doi.org/10.1029/2007JD008459

European Centre for Medium-Range Weather Forecasts (ECMWF). (n.d.). GRIB parameter 235009: Surface total precipitation. Retrieved from https://codes.ecmwf.int/grib/param-db/235009

Feinberg, A., Sukhodolov, T., Luo, B.-P., Rozanov, E., Winkel, L. H. E., Peter, T., & Stenke, A. (2019). Improved tropospheric and stratospheric sulfur cycle in the aerosol–chemistry–climate model SOCOL-AERv2. *Geoscientific Model Development*, *12*(9), 3863–3887. https://doi.org/10.5194/gmd-12-3863-2019

Fueglistaler, S., Dessler, A. E., Dunkerton, T. J., Folkins, I., Fu, Q., & Mote, P. W. (2009). Tropical tropopause layer. *Reviews of Geophysics*, *47*(1). https://doi.org/10.1029/2008RG000267

Gettelman, A., Mills, M. J., Kinnison, D. E., Garcia, R. R., Smith, A. K., Marsh, D. R., et al. (2019). The Whole Atmosphere Community Climate Model Version 6 (WACCM6). *Journal of Geophysical Research: Atmospheres*, *124*(23), 12380–12403. https://doi.org/10.1029/2019JD030943

Geum, S., Park, H., Choi, H., Kim, Y., Lee, H., Joo, S., et al. (2024). Identifying emission sources of CH4 in East Asia based on in-situ observations of atmospheric δ13C-CH4 and C2H6. *Science of the Total Environment*, *908*, 168433. https://doi.org/10.1016/j.scitotenv.2023.168433

Glatthor, N., Höpfner, M., Leyser, A., Stiller, G. P., von Clarmann, T., Grabowski, U., et al. (2017). Global carbonyl sulfide (OCS) measured by MIPAS/Envisat during 2002–2012. *Atmospheric Chemistry and Physics*, *17*(4), 2631–2652. https://doi.org/10.5194/acp-17-2631-2017

Gurganus, C., Feng, W., & Chipperfield, M. P. (2024). TOMCAT ERA5 model data [Dataset]. *NOAA Chemical Sciences Laboratory*. https://csl.noaa.gov/groups/csl6/measurements/data/2024-Gurganus-etal/

Hannigan, J. W., Ortega, I., Shams, S. B., Blumenstock, T., Campbell, J. E., Conway, S., et al. (2022). Global atmospheric OCS trend analysis from 22 NDACC stations. *Journal of Geophysical Research: Atmospheres*, *127*(4), e2021JD035764. https://doi.org/10.1029/2021JD035764

Hattori, S., Kamezaki, K., & Yoshida, N. (2020). Constraining the atmospheric OCS budget from sulfur isotopes. *Proceedings of the National Academy of Sciences*, *117*(34), 20447–20452. https://doi.org/10.1073/pnas.2007260117

Hersbach, H., Bell, B., Berrisford, P., Hirahara, S., Horányi, A., Muñoz-Sabater, J., et al. (2020). The ERA5 global reanalysis. *Quarterly Journal of the Royal Meteorological Society*, *146*(730), 1999–2049. https://doi.org/10.1002/qj.3803

Hoffmann, L., Konopka, P., Clemens, J., & Vogel, B. (2023). Lagrangian transport simulations using the extreme convection parameterization: An assessment for the ECMWF reanalyses. *Atmospheric Chemistry and Physics*, *23*(13), 7589–7609. https://doi.org/10.5194/acp-23-7589-2023

Hoffmann, L., & Spang, R. (2022). An assessment of tropopause characteristics of the ERA5 and ERA-Interim meteorological reanalyses. *Atmospheric Chemistry and Physics*, *22*(6), 4019–4046. https://doi.org/10.5194/acp-22-4019-2022

Honomichl, S. (2023). ACCLIP NSF/NCAR GV instrument data merges - TOGA-based. Version 1.0 (version 1.0) [ICT: NASA ICARTT format, NetCDF: Network Common Data Form (application/x-netcdf)]. UCAR/NCAR - Earth Observing Laboratory. https://doi.org/10.26023/9TJ3-DT16-VZ00

Hoskins, B. J., & Rodwell, M. J. (1995). A model of the Asian summer monsoon. Part I: The global scale. *Journal of the Atmospheric Sciences*, *52*(9), 1329–1340. https://doi.org/10.1175/1520-0469(1995)052<1329:amotas>2.0.co;2

Hu, L., Montzka, S. A., Kaushik, A., Andrews, A. E., Sweeney, C., Miller, J., et al. (2021). COS-derived GPP relationships with temperature and light help explain high-latitude atmospheric CO2 seasonal cycle amplification. *Proceedings of the National Academy of Sciences of the United States of America*, *118*(33), e2103423118. https://doi.org/10.1073/pnas.2103423118

Janowiak, J., Joyce, B., & Xie, P. (2017). [dataset], *NCEP/CPC L3 half hourly 4km global (60S - 60N) merged IR V1*. In A. Savtchenko (Ed.). Goddard Earth Sciences Data and Information Services Center (GES DISC). https://doi.org/10.5067/P4HZB9N27EKU

Jernigan, C. M., Fite, C. H., Vereecken, L., Berkelhammer, M. B., Rollins, A. W., Rickly, P. S., et al. (2022). Efficient production of carbonyl sulfide in the low-NOx oxidation of dimethyl sulfide. *Geophysical Research Letters*, *49*(3), e2021GL096838. https://doi.org/10.1029/2021GL096838

Karu, E., Li, M., Ernle, L., Brenninkmeijer, C. A. M., Lelieveld, J., & Williams, J. (2023). Carbonyl sulfide (OCS) in the upper troposphere/lowermost stratosphere (UT/LMS) region: Estimates of lifetimes and fluxes. *Geophysical Research Letters*, *50*(19), e2023GL105826. https://doi.org/10.1029/2023GL105826

Kettle, A. J., Kuhn, U., von Hobe, M., Kesselmeier, J., & Andreae, M. O. (2002). Global budget of atmospheric carbonyl sulfide: Temporal and spatial variations of the dominant sources and sinks. *Journal of Geophysical Research*, *107*(D22). ACH 25-1–ACH 25-16. https://doi.org/10.1029/2002JD002187

Kloss, C., von Hobe, M., Höpfner, M., Walker, K. A., Riese, M., Ungermann, J., et al. (2019). Sampling bias adjustment for sparsely sampled satellite measurements applied to ACE-FTS carbonyl sulfide observations. *Atmospheric Measurement Techniques*, *12*(4), 2129–2138. https://doi.org/10.5194/amt-12-2129-2019

Kremser, S., Thomason, L. W., von Hobe, M., Hermann, M., Deshler, T., Timmreck, C., et al. (2016). Stratospheric aerosol—Observations, processes, and impact on climate. *Reviews of Geophysics*, *54*(2), 278–335. https://doi.org/10.1002/2015RG000511

Kuai, L., Worden, J., Kulawik, S. S., Montzka, S. A., & Liu, J. (2014). Characterization of Aura TES carbonyl sulfide retrievals over ocean. *Atmospheric Measurement Techniques*, *7*(1), 163–172. https://doi.org/10.5194/amt-7-163-2014

Launois, T., Belviso, S., Bopp, L., Fichot, C. G., & Peylin, P. (2015). A new model for the global biogeochemical cycle of carbonyl sulfide – Part 1: Assessment of direct marine emissions with an oceanic general circulation and biogeochemistry model. *Atmospheric Chemistry and Physics*, *15*(5), 2295–2312. https://doi.org/10.5194/acp-15-2295-2015

Launois, T., Peylin, P., Belviso, S., & Poulter, B. (2015). A new model of the global biogeochemical cycle of carbonyl sulfide – Part 2: Use of carbonyl sulfide to constrain gross primary productivity in current vegetation models. *Atmospheric Chemistry and Physics*, *15*(16), 9285–9312. https://doi.org/10.5194/acp-15-9285-2015

Legras, B., & Bucci, S. (2020). Confinement of air in the Asian monsoon anticyclone and pathways of convective air to the stratosphere during the summer season. *Atmospheric Chemistry and Physics*, *20*(18), 11045–11064. https://doi.org/10.5194/acp-20-11045-2020

Li, D., Vogel, B., Müller, R., Bian, J., Günther, G., Ploeger, F., et al. (2020). Dehydration and low ozone in the tropopause layer over the Asian monsoon caused by tropical cyclones: Lagrangian transport calculations using ERA-Interim and ERA5 reanalysis data. *Atmospheric Chemistry and Physics*, *20*(7), 4133–4152. https://doi.org/10.5194/acp-20-4133-2020

Li, J., Shen, L., Zhang, Y., Liu, Y., Wu, J., & Wang, A. (2024). Carbonyl sulfide (COS) in terrestrial ecosystem: What we know and what we do not. *Atmosphere*, *15*(7), 778. https://doi.org/10.3390/atmos15070778

Ma, J., Kooijmans, L. M. J., Cho, A., Montzka, S. A., Glatthor, N., Worden, J. R., et al. (2021). Inverse modelling of carbonyl sulfide: Implementation, evaluation and implications for the global budget. *Atmospheric Chemistry and Physics*, *21*(5), 3507–3529. https://doi.org/10.5194/acp-21-3507-2021

Montzka, S. A., Calvert, P., Hall, B. D., Elkins, J. W., Conway, T. J., Tans, P. P., & Sweeney, C. (2007). On the global distribution, seasonality, and budget of atmospheric carbonyl sulfide (COS) and some similarities to CO2. *Journal of Geophysical Research*, *112*(D9). https://doi.org/10.1029/2006JD007665

Morrison, H., Morales, A., & Villanueva-Birriel, C. (2015). Concurrent sensitivities of an idealized deep convective storm to parameterization of microphysics. *Horizontal Grid Resolution, and Environmental Static Stability*, *143*(6), 2082–2104. https://doi.org/10.1175/MWR-D-14-00271.1

NASA/LARC/SD/ASDC. (2022). KORUS-AQ aircraft merge data files [dataset], NASA Langley Atmospheric Science Data Center DAAC. https://doi.org/10.5067/ASDC/SUBORBITAL/KORUSAQ_Merge_Data_1

NASA/LARC/SD/ASDC. (2024). ACCLIP WB-57 aircraft merge data [dataset], NASA Langley Atmospheric Science Data Center DAAC. https://doi.org/10.5067/ASDC/SUBORBITAL/ACCLIP_Merge_WB-57-Aircraft_Data_1

National Centers for Environmental Prediction/National Weather Service/NOAA/U.S. Department of Commerce. (1995). NCEP/NCAR global reanalysis 8-day forecast products (updated quarterly) [dataset], Research Data Archive at the National Center for Atmospheric Research, Computational and Information Systems Laboratory. https://doi.org/10.5065/KHX2-FJ42

Network for the Detection of Atmospheric Composition Change (NDACC). (n.d.). FTIR spectrometer data [Dataset]. Retrieved from https://ndacc.larc.nasa.gov/instruments/ftir-spectrometer

Pan, L. L., Atlas, E. L., Honomichl, S. B., Smith, W. P., Kinnison, D. E., Solomon, S., et al. (2024). East Asian summer monsoon delivers large abundances of very short-lived organic chlorine substances to the lower stratosphere. *Proceedings of the National Academy of Sciences*, *121*(12), e2318716121. https://doi.org/10.1073/pnas.2318716121

Pan, L. L., Honomichl, S. B., Kinnison, D. E., Abalos, M., Randel, W. J., Bergman, J. W., & Bian, J. (2016). Transport of chemical tracers from the boundary layer to stratosphere associated with the dynamics of the Asian summer monsoon. *Journal of Geophysical Research: Atmospheres*, *121*(23), 14159–14174. https://doi.org/10.1002/2016JD025616

Pan, L. L., Kinnison, D., Liang, Q., Chin, M., Santee, M. L., Flemming, J., et al. (2022). A multimodel investigation of Asian summer monsoon UTLS transport over the western pacific. *Journal of Geophysical Research: Atmospheres*, *127*(24), e2022JD037511. https://doi.org/10.1029/2022JD037511

Parazoo, N. C., Bowman, K., Fisher, J. B., Frankenberg, C., Jones, D. B. A., Cescatti, A., et al. (2014). Terrestrial gross primary production inferred from satellite fluorescence and vegetation models. *Global Change Biology*, *20*(10), 3103–3121. https://doi.org/10.1111/gcb.12652

Park, H., Kim, J., Choi, H., Geum, S., Kim, Y., Thompson, R. L., et al. (2023). A rise in HFC-23 emissions from eastern Asia since 2015. *Atmospheric Chemistry and Physics*, *23*(16), 9401–9411. https://doi.org/10.5194/acp-23-9401-2023

Park, M., Randel, W. J., Emmons, L. K., Bernath, P. F., Walker, K. A., & Boone, C. D. (2008). Chemical isolation in the Asian monsoon anticyclone observed in Atmospheric Chemistry Experiment (ACE-FTS) data. *Atmospheric Chemistry and Physics*, *8*(3), 757–764. https://doi.org/10.5194/acp-8-757-2008

Park, S., Western, L. M., Saito, T., Redington, A. L., Henne, S., Fang, X., et al. (2021). A decline in emissions of CFC-11 and related chemicals from eastern China. *Nature*, *590*(7846), 433–437. https://doi.org/10.1038/s41586-021-03277-w

Pfister, L., Ueyama, R., Jensen, E. J., & Schoeberl, M. R. (2022). Deep convective cloud top altitudes at high temporal and spatial resolution. *Earth and Space Science*, *9*(11), e2022EA002475. https://doi.org/10.1029/2022EA002475

Ploeger, F., Konopka, P., Walker, K., & Riese, M. (2017). Quantifying pollution transport from the Asian monsoon anticyclone into the lower stratosphere. *Atmospheric Chemistry and Physics*, *17*(11), 7055–7066. https://doi.org/10.5194/acp-17-7055-2017

Plumb, R. A. (1996). A "tropical pipe" model of stratospheric transport. *Journal of Geophysical Research*, *101*(D2), 3957–3972. https://doi.org/10.1029/95JD03002

Randel, W. J., Park, M., Emmons, L., Kinnison, D., Bernath, P., Walker, K. A., et al. (2010). Asian monsoon transport of pollution to the stratosphere. *Science*, *328*(5978), 611–613. https://doi.org/10.1126/science.1182274

Rollins, A. W., Thornberry, T. D., Watts, L. A., Yu, P., Rosenlof, K. H., Mills, M., et al. (2017). The role of sulfur dioxide in stratospheric aerosol formation evaluated by using in situ measurements in the tropical lower stratosphere. *Geophysical Research Letters*, *44*(9), 4280–4286. https://doi.org/10.1002/2017GL072754

Sander, R. (2023). Compilation of Henry's law constants (version 5.0.0) for water as solvent. *Atmospheric Chemistry and Physics*, *23*(19), 10901–12440. https://doi.org/10.5194/acp-23-10901-2023

Schmidt, M., Bernath, P., Boone, C., Lecours, M., & Steffen, J. (2024). Trends in atmospheric composition between 2004–2023 using version 5 ACE-FTS data. *Journal of Quantitative Spectroscopy and Radiative Transfer*, *325*, 109088. https://doi.org/10.1016/j.jqsrt.2024.109088

Schuck, T. J., Blank, A.-K., Rittmeier, E., Williams, J., Brenninkmeijer, C. A. M., Engel, A., & Zahn, A. (2020). Stability of halocarbons in air samples stored in stainless-steel canisters. *Atmospheric Measurement Techniques*, *13*(1), 73–84. https://doi.org/10.5194/amt-13-73-2020

SCISAT Team. (n.d.). ACE-FTS version 5.2 level 2 data [dataset]. https://databace.scisat.ca/level2/ace_v5.2/display_data.php https://databace.scisat.ca/l2signup.php

Serio, C., Montzka, S. A., Masiello, G., & Carbone, V. (2023). Trend and multi-frequency analysis through empirical mode decomposition: An application to a 20-year record of atmospheric carbonyl sulfide measurements. *Journal of Geophysical Research: Atmospheres*, *128*(3), e2022JD038207. https://doi.org/10.1029/2022JD038207

Sheng, J.-X., Weisenstein, D. K., Luo, B.-P., Rozanov, E., Stenke, A., Anet, J., et al. (2015). Global atmospheric sulfur budget under volcanically quiescent conditions: Aerosol-chemistry-climate model predictions and validation. *Journal of Geophysical Research: Atmospheres*, *120*(1), 256–276. https://doi.org/10.1002/2014JD021985

Simayi, M., Shi, Y., Xi, Z., Ren, J., Hini, G., & Xie, S. (2022). Emission trends of industrial VOCs in China since the clean air action and future reduction perspectives. *Science of the Total Environment*, *826*, 153994. https://doi.org/10.1016/j.scitotenv.2022.153994

Simpson, I. J., Blake, D. R., Blake, N. J., Meinardi, S., Barletta, B., Hughes, S. C., et al. (2020). Characterization, sources and reactivity of volatile organic compounds (VOCs) in Seoul and surrounding regions during KORUS-AQ. *Elementa: Science of the Anthropocene*, *8*, 37. https://doi.org/10.1525/elementa.434

Smith, W., Ueyama, R., & Honomichl, S. (2023). Trajectory-derived convective influence for ACCLIP airborne in situ observations (Version 1.1) [NetCDF: Network Common Data Form (application/x-netcdf),ICT: NASA ICARTT format]. UCAR/NCAR - Earth Observing Laboratory. https://doi.org/10.26023/DP1P-C32K-YJ05

Smith, W. P., Pan, L. L., Kinnison, D., Atlas, E., Honomichl, S., Zhang, J., et al. (2024). Evaluating the model representation of Asian summer monsoon upper troposphere and lower stratosphere transport and composition using airborne in situ observations. *Journal of Geophysical Research: Atmospheres*, *129*(4), e2023JD039756. https://doi.org/10.1029/2023JD039756

Smith, W. P., Pan, L. L., Ueyama, R., Honomichl, S., Campos, T., Viciani, S., et al. (2025). Transport by Asian summer monsoon convection to the upper troposphere and lower stratosphere during ACCLIP (2022). *Journal of Geophysical Research: Atmospheres*, *130*(7), e2024JD042732. https://doi.org/10.1029/2024JD042732

Stein, A. F., Draxler, R. R., Rolph, G. D., Stunder, B. J. B., Cohen, M. D., & Ngan, F. (2015). NOAA's HYSPLIT atmospheric transport and dispersion modeling system [Software]. *NOAA Air Resources Laboratory*. https://doi.org/10.1175/BAMS-D-14-00110.1

Taha, G., Loughman, R., Zhu, T., Thomason, L., Kar, J., Rieger, L., & Bourassa, A. (2021). OMPS LP Version 2.0 multi-wavelength aerosol extinction coefficient retrieval algorithm. *Atmospheric Measurement Techniques*, *14*(2), 1015–1036. https://doi.org/10.5194/amt-14-1015-2021

Tiedtke, M. (1989). A comprehensive mass flux scheme for cumulus parameterization in large-scale models. *Monthly Weather Review*, *117*(8), 1779–1800. https://doi.org/10.1175/1520-0493(1989)117<1779:acmfsf>2.0.co;2

Tilmes, S., Mills, M. J., Zhu, Y., Bardeen, C. G., Vitt, F., Yu, P., et al. (2023). Description and performance of a sectional aerosol microphysical model in the Community Earth System Model (CESM2). *Geoscientific Model Development*, *16*(21), 6087–6125. https://doi.org/10.5194/gmd-16-6087-2023

Treadaway, V., Atlas, E., Schauffler, S., Navarro, M., Ueyama, R., Pfister, L., et al. (2022). Long-range transport of Asian emissions to the West Pacific tropical tropopause layer. *Journal of Atmospheric Chemistry*, *79*(2), 81–100. https://doi.org/10.1007/s10874-022-09430-7

Vogel, B., Müller, R., Günther, G., Spang, R., Hanumanthu, S., Li, D., et al. (2019). Lagrangian simulations of the transport of young air masses to the top of the Asian monsoon anticyclone and into the tropical pipe. *Atmospheric Chemistry and Physics*, *19*(9), 6007–6034. https://doi.org/10.5194/acp-19-6007-2019

Wang, W., Tian, Y., Liu, C., Sun, Y., Liu, W., Xie, P., et al. (2017). Investigating the performance of a greenhouse gas observatory in Hefei, China. *Atmospheric Measurement Techniques*, *10*(7), 2627–2643. https://doi.org/10.5194/amt-10-2627-2017

Yan, X., Konopka, P., Ploeger, F., Podglajen, A., Wright, J. S., Müller, R., & Riese, M. (2019). The efficiency of transport into the stratosphere via the Asian and North American summer monsoon circulations. *Atmospheric Chemistry and Physics*, *19*(24), 15629–15649. https://doi.org/10.5194/acp-19-15629-2019

Yan, Y., Li, R., Peng, L., Yang, C., Liu, C., Cao, J., et al. (2019). Emission inventory of carbonyl sulfide (COS) from primary anthropogenic sources in China. *Environmental Pollution*, *247*, 745–751. https://doi.org/10.1016/j.envpol.2019.01.096

Yujing, M., Hai, W., Zhang, X., & Jiang, G. (2002). Impact of anthropogenic sources on carbonyl sulfide in Beijing City. *Journal of Geophysical Research*, *107*(D24). ACH 13-1–ACH 13-7. https://doi.org/10.1029/2002JD002245

Zumkehr, A., Hilton, T. W., Whelan, M., Smith, S., Kuai, L., Worden, J., & Campbell, J. E. (2018). Global gridded anthropogenic emissions inventory of carbonyl sulfide. *Atmospheric Environment*, *183*, 11–19. https://doi.org/10.1016/j.atmosenv.2018.03.063